

## RESEARCH ARTICLE

10.1029/2021JD035419

### Key Points:

- Total particle number concentrations (PNCs) decreased by 5% in 2016–2018 relative to 2010–2012, despite the PM<sub>2.5</sub> decreased by over 40%
- In 2016–2018, nucleation-mode PNCs decreased by 20% relative to 2010–2012, whereas accumulation-mode PNCs increased by 11%
- Maximum sizes of grown new particles were reduced by 50%, leading to a decreased contribution of new particles to accumulation mode PNCs

### Supporting Information:

Supporting Information may be found in the online version of this article.

### Correspondence to:

X. Yao and L. Xue,  
[xhyao@ouc.edu.cn](mailto:xhyao@ouc.edu.cn);  
[xuelikun@sdu.edu.cn](mailto:xuelikun@sdu.edu.cn)

### Citation:

Zhu, Y., Shen, Y., Li, K., Meng, H., Sun, Y., Yao, X., et al. (2021). Investigation of particle number concentrations and new particle formation with largely reduced air pollutant emissions at a coastal semi-urban site in northern China. *Journal of Geophysical Research: Atmospheres*, 126, e2021JD035419. <https://doi.org/10.1029/2021JD035419>

Received 17 JUN 2021  
 Accepted 20 AUG 2021

### Author Contributions:

**Conceptualization:** Xiaohong Yao

**Data curation:** Yujiao Zhu

**Formal analysis:** Yujiao Zhu, He Meng, Yue Sun

**Funding acquisition:** Xiaohong Yao, Likun Xue

**Investigation:** Yujiao Zhu, Yanjie Shen, Kai Li

**Project Administration:** Xiaohong Yao, Huiwang Gao

**Supervision:** Huiwang Gao, Wenxing Wang

**Writing – original draft:** Yujiao Zhu

**Writing – review & editing:** Xiaohong Yao, Likun Xue

© 2021. American Geophysical Union.  
 All Rights Reserved.

# Investigation of Particle Number Concentrations and New Particle Formation With Largely Reduced Air Pollutant Emissions at a Coastal Semi-Urban Site in Northern China

Yujiao Zhu<sup>1,2</sup> , Yanjie Shen<sup>2</sup>, Kai Li<sup>3</sup>, He Meng<sup>4</sup>, Yue Sun<sup>1</sup>, Xiaohong Yao<sup>2,5</sup> , Huiwang Gao<sup>2,5</sup> , Likun Xue<sup>1,6</sup> , and Wenxing Wang<sup>1</sup>

<sup>1</sup>Environment Research Institute, Shandong University, Qingdao, China, <sup>2</sup>Key Laboratory of Marine Environment and Ecology, and Frontiers Science Center for Deep Ocean Multispheres and Earth System, Ministry of Education, Ocean University of China, Qingdao, China, <sup>3</sup>Centre for Sustainable Development and Energy Policy Research, School of Energy and Mining Engineering, China University of Mining & Technology, Beijing, China, <sup>4</sup>Qingdao Eco-environment Monitoring Center of Shandong Province, Qingdao, China, <sup>5</sup>Laboratory for Marine Ecology and Environmental Sciences, Qingdao National Laboratory for Marine Science and Technology, Qingdao, China, <sup>6</sup>Collaborative Innovation Center for Climate Change, Nanjing, China

**Abstract** To better understand the responses of particle number concentrations (PNCs) and new particle formation (NPF) to the largely reduced air pollutant emissions in urban atmospheres, we investigated the particle number size distributions in Qingdao, a coastal megacity in northern China, during two separate periods, 2010–2012 and 2016–2018. The results show only an average of 5% decrease in the total PNCs in 2016–2018 relative to 2010–2012, although the PM<sub>2.5</sub> mass concentration decreased by over 40%. Nucleation-mode PNCs decreased by 20%, which is attributable to reductions in primary emissions from on-road vehicles and secondary sources. Unexpectedly, the accumulation-mode PNCs increased by 11% in 2016–2018 relative to 2010–2012. The SO<sub>2</sub> concentrations strongly decreased by ~60%, and the NPF frequencies slightly decreased from 34% in 2010–2012 to 25% in 2016–2018. However, there were no significant changes in the apparent new particle formation rate (FR) or net maximum increase in nucleation-mode PNCs (NMINP). The increased concentrations of other precursors may substantially negate the effect of SO<sub>2</sub> reduction, leading to the invariant FR and NMINP. The maximum sizes of grown new particles decreased by 50%; combined with the decreased NPF frequency, the contribution of grown new particles to accumulation-mode PNCs expectedly decreased in 2016–2018 relative to 2010–2012. Alternatively, the increased accumulation-mode PNCs in 2016–2018 mainly attribute to the enhanced primary combustion emissions excluding on-road vehicle emissions. The increase in accumulation-mode PNCs in 2016–2018 provides insights on the inter-annual variation in satellite-based cloud properties, which appeared insensitive to the large decrease in satellite-based aerosol optical depth.

## 1. Introduction

Atmospheric particles play an important role in modifying the Earth's radiative balance, degrading visibility, and adversely affecting human health (Charlson et al., 1992; Heal et al., 2012; IPCC, 2013; Kulmala et al., 2021; R. Zhang et al., 2015). Particle number concentrations (PNCs) and particle number size distributions (PNSDs) in ambient air are essential to evaluate climate effects, characterize human exposure, and formulate relevant protection policies (Dusek et al., 2006; Kumar et al., 2010; Vu et al., 2015). For example, atmospheric particles with a diameter <50 nm reportedly act as cloud condensation nuclei (CCN) in exceptionally high supersaturation (SS) conditions, such as >0.6%, whereas particles with a diameter >80 nm significantly contribute to the CCN population at SS conditions of ~0.2% (Dusek et al., 2006; Kerminen et al., 2018; K. Li et al., 2015; N. Ma et al., 2016; Petters & Kreidenweis, 2007; Wiedensohler et al., 2009; Yue et al., 2011; Zhu et al., 2019). Atmospheric particles with a diameter >100 nm can yield detectable direct climate impacts by scattering and absorbing solar radiation (Charlson et al., 1992; Seinfeld & Pandis, 2012). Smaller nanometer-scale atmospheric particles, meanwhile, may cause greater adverse health outcomes than larger particles (Schlesinger et al., 2006; R. Zhang et al., 2015).

New particle formation (NPF) is regarded as an important secondary source of atmospheric particles on a global scale in terms of number concentrations (Kerminen et al., 2018; Kulmala & Kerminen, 2008; Kulmala et al., 2013; S. H. Lee et al., 2019; R. Zhang et al., 2012). Sulfuric acid is commonly considered as the key nucleating precursor for NPF, whereas other species, such as ammonia, amines, and highly oxygenated molecules (HOMs), can also participate in and enhance nucleation in the continental troposphere (Ehn et al., 2014; S. H. Lee et al., 2019; Tröstl et al., 2016; L. Yao et al., 2018). Iodine oxides have been reported to induce NPF in some coastal zones and sea-ice regions (e.g., O'Dowd et al., 2002; Sipilä et al., 2016; Yu et al., 2019). Freshly nucleated particles can subsequently grow to larger sizes, a process that has been proposed to be driven by low-volatility gaseous species (e.g., sulfuric acid, HOMs) together with semi-volatile compounds (e.g., ammonium nitrate, small molecule secondary organic compounds) (Ehn et al., 2014; Man et al., 2015; Riipinen et al., 2012; Tröstl et al., 2016; Wang, Kong, et al., 2020; Zhu et al., 2014).

PNCs and PNSDs in remote clean atmospheres have been well studied in recent decades in terms of primary origins, ambient nucleation, subsequent growth of newly formed particles, and associated indirect climate impacts via ground-based and aircraft-based measurements in different time scales, laboratory experiments, and 3-D modeling on regional and global scales (e.g., Asmi et al., 2011; Bianchi et al., 2016; Gerling et al., 2021; Harrison et al., 2011; Nieminen et al., 2014; Yu & Luo, 2009; Zhu et al., 2002). Several review papers have summarized the achievements and outlined the challenges ahead (Kerminen et al., 2018; Kulmala & Kerminen, 2008; Kumar et al., 2010; S. H. Lee et al., 2019; R. Zhang et al., 2012, 2015). In China, campaign-based studies are also frequently reported, with observational periods varying from several months to 1–2 years (e.g., Chu et al., 2019; Kivekäs et al., 2009; Kulmala et al., 2016, 2021; Qi et al., 2015; X. Shen et al., 2011; Z. B. Wang et al., 2013; Wehner et al., 2004; Wiedensohler et al., 2009; Wu et al., 2007, 2008; L. Yao et al., 2018; Yue et al., 2009; Zhou et al., 2020; Zhu et al., 2017). However, there have been few long-term observations of PNCs, PNSDs and NPF in China in the presence of substantially reduced SO<sub>2</sub> emissions, which restricts our understanding of the responses of PNCs, PNSDs, and NPF to dramatic changes in the concentrations of anthropogenic air pollutants and biogenic volatile organic compounds (VOCs) (M. Liu et al., 2018; C. Zheng et al., 2017; B. Zheng et al., 2018). The same problem applies to the impacts of variable PNCs and PNSDs on public health and regional climate in response to the dramatic emission changes of various anthropogenic and biogenic air pollutants.

Qingdao is a coastal megacity in northern China (Figures 1a and 1b) situated on the transport pathway of continental air pollutants to the northwest Pacific Ocean and even as far as to the Arctic (Shi et al., 2019; C. Zhang et al., 2019). The concentrations of anthropogenic air pollutants have substantially decreased with continuously tightening control policies in the past decades. For example, the annual average SO<sub>2</sub> concentrations in Qingdao decreased by 84% from 2010 to 2019 and PM<sub>2.5</sub> mass concentrations decreased by 44% during 2013–2019 (Figure 1c). The satellite-derived aerosol optical depth (AOD) over Qingdao also showed similar downward trend from 2010 to 2019 (Figure S1). In contrast, biological emissions may change in the opposite direction. China has experienced rapid afforestation in recent decades, resulting in an estimated ~18% net increase in leaf area (C. Chen et al., 2019; Wang, Feng, et al., 2020). Meanwhile, the ambient temperature in Qingdao has increased at a rate of 0.17°C/year ( $p < 0.01$ ) (Figure S2a). The emission of biogenic organic compounds is reasonably expected to increase owing to the increased forest area and accelerating global warming (W. H. Chen et al., 2018; H. Wang et al., 2021; Wang, Feng, et al., 2020; X. D. Zhang et al., 2016). Research in Qingdao not only provides updated knowledge to service local issues, but is also important for understanding the related influence of long-range transport on the downwind atmosphere.

In this study, PNC and PNSD observations were conducted at a semi-urban site in Qingdao from 2010 onward. Data measured during two separate periods, 2010–2012 and 2016–2018, were used for comparative analysis. The objectives of this study are to (a) determine the overall response of PNCs and PNSDs to large reductions of air pollutant emissions in terms of changed primary and secondary sources; (b) determine the influence of reduced air pollutant emissions on NPF events in terms of the NPF frequency, formation, and growth characteristics; and (c) build on (a) and (b) to understand the response of satellite-based aerosol and cloud data to reduced air pollutant emissions.

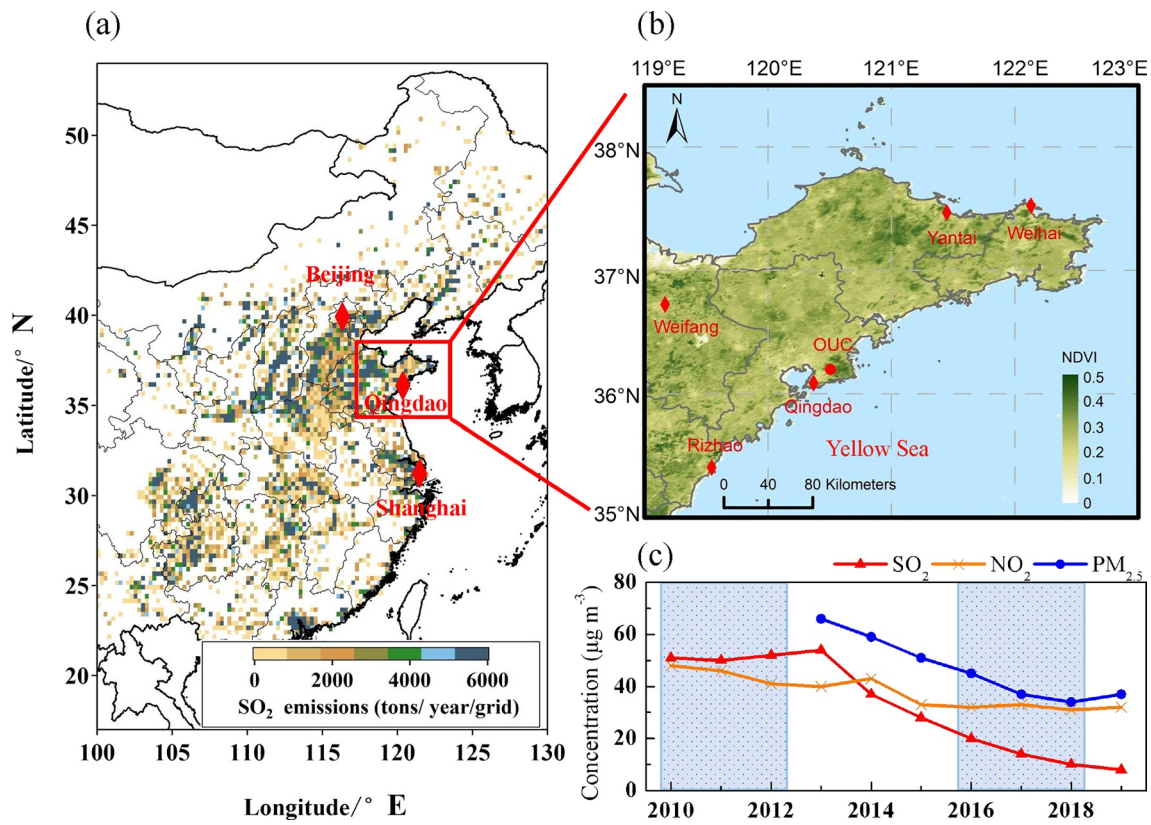


**Figure 1.** The Spatial distribution of anthropogenic SO<sub>2</sub> emissions in China in 2016 (a), location of Ocean University of China (OUC, red circles in (b)) and annual changes in air pollutant concentrations of SO<sub>2</sub>, NO<sub>2</sub>, and PM<sub>2.5</sub> at the sampling site from 2010 to 2019 (c). The SO<sub>2</sub> emissions in (a) were obtained from [www.meicmodel.org](http://www.meicmodel.org). The map in (b) was color-coded by the MODIS-derived normalized difference vegetation index (NDVI) in June 2012. The data in (c) are from the Bulletin of the Ecological Environment in Qingdao City (<http://hbj.qingdao.gov.cn/m2/zwgkSecond.aspx?m=35>).

## 2. Methods

### 2.1. Experimental Protocol

PNSD measurements were carried out at a semi-urban site in Qingdao City (36°09'37"N, 120°29'44"E, Figures 1a and 1b). The site is located on the fifth floor of an academic building on the Laoshan campus of the Ocean University of China, ~7 km from the Yellow Sea coastline and ~10 km from the center of an urban area. The site is ~300 m from a major traffic road with moderately heavy traffic flow (Figure S3). A fast mobility particle sizer (FMPS, TSI Model 3091) has operated semi-continuously downstream of a dryer and recorded the number-based size distribution of atmospheric particles since 2010. Two data sets were used in this study, covering the time intervals of 2010–2012 and 2016–2018 (see Table S1 for details of the valid sampling days). It should be noted that there were no valid sampling days in August, September, and November in 2016–2018, and the data from the same months of 2010–2012 were excluded from analysis to ensure the consistency of the sampling times. Valid data were thus used for 281 and 343 days for the two data sets, respectively. In the remaining time, the FMPS instrument performed field observation experiments on the seas or was calibrated and/or repaired (X. H. Liu et al., 2014; Meng et al., 2015; Zhu et al., 2019). Some parts of the two data sets have been presented in previous studies to distinguish the different growth types of new particles, chemicals driving particle growth, and their CCN activity (K. Li et al., 2015; Zhu et al., 2014, 2019). This study combined all of the available data to evaluate the effects of reduced anthropogenic emissions on the PNSDs and regional NPF events.

The FMPS is a paralleling particle sizer and reports PNSDs from 5.6 to 560 nm with a 1-s time resolution, which can successfully distinguish new particle signals from a mixture of different particle sources (X. H. Liu et al., 2014; Man et al., 2015). However, the underestimation of FMPS has been reported when the measured sizes are larger than 100 nm, compared with data obtained using a scanning mobility particle

sizer (SMPS) and high-resolution time-of-flight aerosol mass spectrometer (B. P. Lee et al., 2013). In this study, the empirical correction procedure for FMPS data proposed by Zimmerman et al. (2015) was used for correction. The upper limit of 523 nm (midpoint) was adjusted to 857 nm (midpoint) following the method of Zimmerman et al. (2015), and the scaling-down coefficient of the total particle number concentrations (t-PNCs) measured using the FMPS was obtained through correlation analysis of side-by-side measurements made by the FMPS and a condensation particle counter (TSI Model 3775). The coefficient varied between 0.75 and 1.28 in different years after each regular annual maintenance (listed in Table S2); according to Zimmerman et al. (2015), however, the coefficient correction did not change PNSD patterns. Comparisons between the measurement performance of the FMPS and the SMPS (TSI Model 3910/Grimm LDMA + CPC) were conducted in 2012 and 2019. Figures S4 and S5 show the high consistency between the PNSDs measured using each of these devices. The minimum particle number concentrations in each size bin measured by FMPS are shown in Table S3. Conductive tubes (TSI 1/4 in.) were used for FMPS sampling, and the length of the tube was ~2 m. The presence or absence of the tube had little influence on the measured total PNCs.

## 2.2. Definition of NPF Events and Calculation Methods

In this study, particles with a diameter smaller than 25 nm were defined as nucleation-mode particles (Kulmala et al., 2012). An NPF event was classified following the criteria proposed by Dal Maso et al. (2005) and Kulmala et al. (2012): (a) a distinctly new nucleation mode must appear in the particle size distribution; (b) the new mode should prevail over a time span of hours (defined as 2 h in this study); and (c) the new mode should show signs of growth.

An NPF event was defined to have initiated at the time when the new nucleation-mode particles became observable. The NPF event was defined to have ended when the new particle signal became negligible and the t-PNCs approached the background levels prior to the NPF event. In the cases involving plume invasions, the end time was determined to be the time when the new particle signals became overwhelmed by plumes and were no longer identifiable. The time duration between the initial and end times of an NPF event was defined as the NPF event duration (Figure S6). The particle signals within the NPF event duration were defined as the NPF category.

We used seven parameters to evaluate the NPF characteristics: NPF frequency; apparent new particle formation rate (FR); growth rate (GR); condensation sink (CS); net maximum increase in the nucleation-mode particle number concentration (NMINP); maximum size of the geometric median diameter of the new particles ( $D_{pgmax}$ ); and the NPF duration (Kulmala et al., 2012; Sihto et al., 2006; Zhu et al., 2019, 2021). FR and NMINP represent the intensity of an NPF event and are calculated based on the nucleation-mode particles in sizes of 5.6–25 nm. GR is quantified by fitting the geometric median diameter of the new particles ( $D_{pg}$ ) during the particle growth period, in which the size range of  $D_{pg}$  varies from event to event. GR and  $D_{pgmax}$  are two indicators of the potential climate impact of new particles. CS is the loss rate of condensable vapor molecules onto pre-existing particles and is calculated based on 10–857 nm particles. Details of the calculation of these parameters can be found in numerous studies (e.g., Kulmala et al., 2012; Sihto et al., 2006; Zhu et al., 2019, 2021) and in the Supporting Information S1.

## 2.3. Determination of Plume and Background Categories of Ambient Particles

Aside from the NPF category, we focused on two other categories of particles: the plume category and the background category. Particles in the plume or background category in the ambient environment were distinguished using the following approach. We first averaged the 1-s time resolution data to a 10-min time resolution, integrated the data of each month into a single file, and removed the time period of the NPF category from the file. We then calculated the t-PNCs based on the size distribution data and rearranged the t-PNC values from smallest to largest to generate a new array of data in a month. For this analysis, we assumed that particles in the low number concentrations were of the background category and used the 0–25th percentile data. Particles in the high number concentrations suggest the invasion of air pollutant plumes; we thus used the 75th–100th percentile data to represent the plume category.

As an alternative approach, we also visually analyzed the FMPS data on a day-to-day basis and subjectively distinguished the plumes and background particles. Figure S7 shows an example of the selected period of plumes and background particles. We plotted the monthly averaged PNSDs of the selected plume category particles and background category particles, and found highly consistent PNSD values between the two approaches, as shown in Figure S8. The difference of the t-PNCs was 12% and 20% for plume category and background category particles, respectively. The first approach was adopted in the following analyses because it enabled the same amount of data to be used for the plume category and background category particles.

### 3. Results

#### 3.1. Comparison of the t-PNC Values Measured Between 2010–2012 and 2016–2018

The t-PNCs took values of  $1.7 \pm 1.1 \times 10^4 \text{ cm}^{-3}$  (average  $\pm$  standard deviation) and  $1.6 \pm 1.0 \times 10^4 \text{ cm}^{-3}$  during 2010–2012 and 2016–2018, respectively. The two averages are essentially the same, although the annual average  $\text{PM}_{2.5}$  mass concentrations in Qingdao decreased by more than 40% between the two periods (Figure 1c). It is surprising to find that the previously reported campaign-based averages and annual averages of t-PNC in some urban or suburban atmospheres over semi-humid and humid areas of China narrowed at  $1.6\text{--}1.7 \times 10^4 \text{ cm}^{-3}$  within 20% margins (Huang et al., 2017; S. Liu et al., 2008; Peng et al., 2014; Qi et al., 2015; L. Shen et al., 2016; X. Shen et al., 2011). In contrast, the averages nearly doubled ( $2.9\text{--}3.3 \times 10^4 \text{ cm}^{-3}$ ) in urban atmospheres over semi-arid and arid urban areas of China (e.g., Beijing and Urumchi), possibly because of reduced wet deposition and a higher occurrence frequency of NPF events (L. Ma et al., 2021; Peng et al., 2014; Wu et al., 2008). The t-PNC values in the nonheating season (April to October) and heating season (November to March in the following year) were also compared separately. In each season, the averaged t-PNCs were generally similar in the two periods. For example, the average t-PNCs in the nonheating season were  $1.4 \pm 1.0 \times 10^4 \text{ cm}^{-3}$  in 2010–2012 and  $1.3 \pm 0.9 \times 10^4 \text{ cm}^{-3}$  in 2016–2018. In the heating season, the average t-PNCs were  $2.0 \pm 1.1 \times 10^4 \text{ cm}^{-3}$  in 2010–2012 and  $1.8 \pm 0.9 \times 10^4 \text{ cm}^{-3}$  in 2016–2018.

Two well-recognized and important contributors to t-PNCs in urban atmospheres are (a) that on-road vehicle emissions mostly dominate the t-PNC values in the morning and late afternoon rush hours, and (b) that NPF sometimes dominate t-PNC values at 08:00–13:00 LT (local time, UTC+8) (Peng et al., 2014; Vu et al., 2015; Zhou et al., 2020; Zhu et al., 2014). The diurnal variations in the hourly average t-PNCs in 2010–2012 and 2016–2018 are compared in Figure 2a. In each of the two 24-h periods, the hourly average t-PNCs fell to their lowest level before 05:00 LT. The hourly average values at each hour before 05:00 LT in 2016–2018 were consistently larger ( $7\% \pm 3\%$ ) than the corresponding values in 2010–2012. After 06:00 LT, an evident increase in t-PNC can be found in both periods with the daily maximum hourly average t-PNC occurring at 09:00 LT in 2010–2012 and 08:00 LT in 2016–2018. The maximum percentage increase in the hourly average t-PNC in the morning rush hours reached 100% in 2010–2012, but was only 52% in 2016–2018. This led to hourly averages in 2016–2018 that were 17% at 08:00 LT and 23% at 09:00 LT smaller than the corresponding values in 2010–2012. The hourly average t-PNCs in 2010–2012 fell to their second lowest level after 17:00 LT. However, in 2016–2018, no clear decrease in hourly average t-PNC occurred at 17:00–23:00 LT relative to those at 06:00–16:00 LT. As a result, the hourly average t-PNCs at each hour after 17:00 LT in 2016–2018 were consistently higher ( $8\% \pm 4\%$ ) than the corresponding values in 2010–2012. A separate analysis of the data in nonheating and heating seasons (Figures S9a and S9c) showed that there were generally higher hourly average t-PNCs in the daytime and lower hourly average t-PNCs at nighttime in 2010–2012 relative to those in 2016–2018. There was also a slight difference between the diurnal variation patterns of t-PNC in the nonheating and heating seasons, probably due to the combined effects of sunrise time, the mixing layer height, and NPF events, among other factors.

No long-term traffic flow data from the major road near the sampling site were available. Short-term records and statistical data were used for the analysis. In December 2020, the on-site counted traffic flows reached 4500–5500 vehicles per hour on weekday morning (07:00–08:00) and afternoon (17:00–18:00) rush hours, which was 1.6 times higher than the counted traffic densities in December 2015 (Teng et al., 2017). Note that normal working hours start from 08:00 LT in China. In addition, the reported vehicle population in Qingdao was 29 per 100 households in 2012 and increased to 54 per 100 households in 2016 (sourced from Qingdao

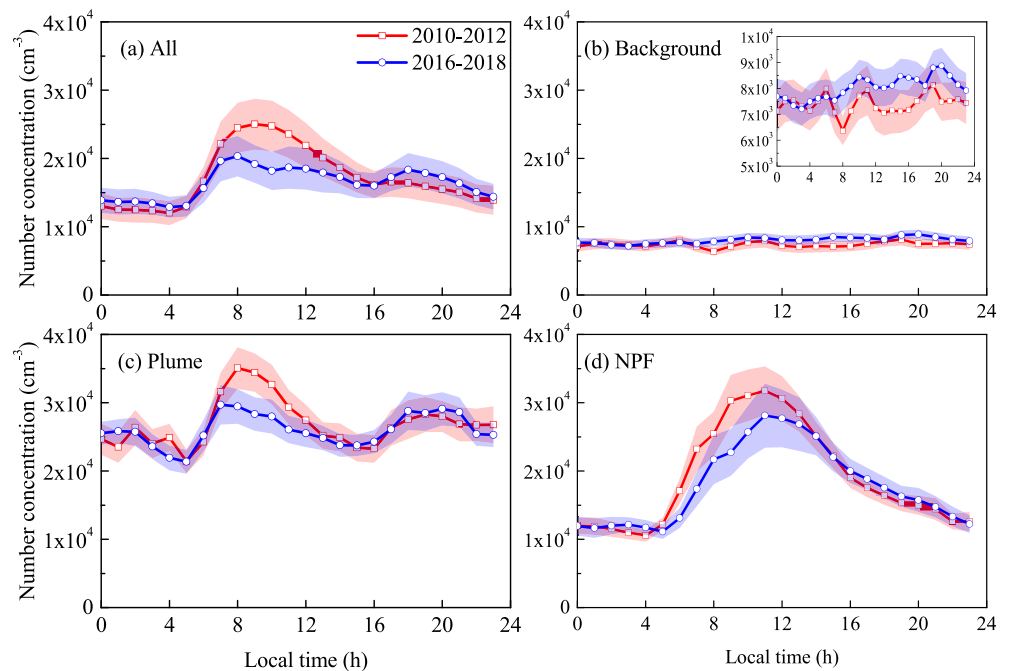


**Figure 2.** Average diurnal variations of particle number concentrations of overall particles (a), background category particles (b), plume category particles (c), and new particle formation category particles (d) in 2010–2012 (red) and 2016–2018 (blue). Shaded areas represent a quarter of the standard deviations.

Statistical Bulletin, <http://qdtj.qingdao.gov.cn/n28356045/n32561056/n32561072/index.html>). However, in 2014 and 2015, Qingdao implemented a program to eliminate on-road vehicles with high air pollutant emissions (Bulletin of the Ecological Environment in Qingdao City in 2015). This may have led to the lower morning t-PNC peak in 2016–2018 than in 2010–2012, although the on-road traffic flow was presumably substantially higher in 2016–2018.

The diurnal variations in the hourly average t-PNC values between the two periods were further compared to distinguish three categories: background, plume, and NPF. In the background category (Figure 2b), there were no evident diurnal variations in both 2010–2012 and 2016–2018. Before 08:00 LT, no consistent trend in hourly average t-PNC can be obtained from an hour-by-hour comparison between the two periods, that is, the percentage changes of each hourly average in 2016–2018 relative to 2010–2012 varied from  $-8\%$  to  $4\%$ . However, the hourly average t-PNCs after 08:00 LT in 2016–2018 were consistently larger ( $12\% \pm 6\%$ ) than the corresponding values in 2010–2012.

In the plume category (Figure 2c), the bimodal diurnal variation in t-PNC values can be identified. The hourly average t-PNCs at 07:00–12:00 in 2016–2018 were consistently less ( $12\% \pm 5\%$ ) than the corresponding values in 2010–2012. However, no consistent trend in hourly average t-PNC can be obtained from the same comparison at other hours, as the percentage changes of each hourly average in 2016–2018 varied from  $-12\%$  to  $10\%$  relative to 2010–2012.

In the NPF category, a unimodal diurnal variation in t-PNC can be identified with one broad t-PNC peak occurring after 06:00 LT, the maximum t-PNC occurring at 11:00 LT, and a long tail extending to midnight in each of the periods (Figure 2d). NPF events usually start around 08:00–10:00 LT in Qingdao (Zhu et al., 2014). From 08:00 LT to 11:00 LT, the net maximum increase of t-PNCs was the same at  $0.6 \times 10^4 \text{ cm}^{-3}$  in each of the periods. The net maximum increase should thus be mainly due to the secondary formation of atmospheric particles via NPF events. However, the hourly average t-PNCs at 08:00–11:00 LT in 2016–2018 were consistently smaller ( $17\% \pm 6\%$ ) than the corresponding values in 2010–2012 with an absolute difference of  $0.36\text{--}0.75 \times 10^4 \text{ cm}^{-3}$ . This difference may have been caused mainly by the reduced primary emissions of atmospheric particles rather than NPF events. For example, at 06:00–07:00, absent of NPF events,

the hourly average t-PNCs in 2016–2018 were 23%–25% smaller than the corresponding values in 2010–2012 with an absolute difference of  $0.40\text{--}0.58 \times 10^4 \text{ cm}^{-3}$ .

The separation of the nonheating and heating seasons for comparative analysis reduced the data size, which unavoidably resulted in increased uncertainties in the comparison results. Thus, the lower t-PNCs in the nonheating season were used for comparative analysis of the background category, whereas the higher t-PNCs in the heating season were used for comparative analysis of the plume category. Similarly, the NPF events in the nonheating season were used for comparative analysis of the NPF category because of the lower background t-PNCs in this season. In the background category for the nonheating season, the hourly average t-PNCs after 08:00 LT in 2016–2018 were consistently  $22\% \pm 6\%$  greater than the corresponding values in 2010–2012 (Figure S9d). Similarly, the hourly average t-PNCs before 08:00 LT in 2016–2018 were consistently  $10\% \pm 4\%$  greater than the corresponding values in 2010–2012, although no consistent trend in hourly average t-PNC was obtained by combining the data for the heating and nonheating seasons. In the plume category for the heating season, the hourly average t-PNCs in 2016–2018 were consistently  $11\% \pm 5\%$  less than the corresponding values in 2010–2012 (Figure S9b). In the category for the combined heating and nonheating seasons, a consistently  $12\% \pm 5\%$  lower hourly average for the t-PNCs in 2016–2018, relative to 2010–2012, occurred only at 07:00–12:00.

In the NPF category in the nonheating season, the net maximum increase in t-PNCs from 08:00 LT to 11:00 LT was almost the same in each of the periods, as it ranged from  $0.8$  to  $1.0 \times 10^4 \text{ cm}^{-3}$  (Figure S9e). The hourly average t-PNCs at 08:00–11:00 LT in 2016–2018 were also consistently  $22\% \pm 9\%$  less than the corresponding values in 2010–2012. As with the averages obtained from combining the heating and nonheating seasons, this difference may be attributable to the reduced primary emissions of atmospheric particles, as revealed by the comparative analysis of data for 06:00–08:00.

### 3.2. Comparison of PNCs in Different Modes Measured Between 2010–2012 and 2016–2018

The nucleation mode, Aitken mode, and accumulation mode are conventionally used to characterize particle number concentration spectra (Kumar et al., 2010; Vu et al., 2015). Here, the three modes were considered to correspond to particle sizes of  $<25$  nm, 25–100 nm, and  $>100$  nm, respectively. Primary-nucleation mode particles reportedly form through nucleation and rapid particle growth after cooling and dilution of hot gaseous exhausts, whereas secondary-nucleation mode particles are always associated with NPF events (Vu et al., 2015; R. Zhang et al., 2012; Zhu et al., 2017). Aitken-mode particles are either derived from condensational growth, the coagulation of nucleation-mode particles, or emitted directly from combustion sources in the urban atmosphere. Primary combustion emissions and the growth of Aitken-mode particles are two major contributors to accumulation-mode particles (Hoppel et al., 1986; Kumar et al., 2010; Vu et al., 2015; X. H. Yao et al., 2005).

Figures 3a–3c compare the diurnal variations in PNCs of the three particle modes between the two periods. The diurnal pattern of the nucleation-mode PNCs displayed a trimodal distribution in 2016–2018. There were three peaks at 07:00 LT, 12:00 LT, and 17:00 LT, which correspond to morning and afternoon rush hours and NPF events in between. In contrast, a broad unimodal distribution was identified in 2010–2012, peaking at 10:00 LT (Figure 3a). This likely reflected a combination of contributions from different sources, that is, vehicle emissions and NPF events, which overlapped to a greater extent. The increase in nucleation and Aitken mode before 08:00 should be mainly ascribed to primary emissions from on-road vehicles while NPF events became important afterward. However, no unique solution can be obtained to separate the board peak in PNSD mathematically. Before 16:00, the hourly average nucleation-mode PNCs were consistently lower in 2016–2018 than 2010–2012. However, after 16:00, there was no consistent result through the same comparison of PNCs in 2016–2018 with 2010–2012. The maximum difference of the nucleation-mode PNCs between the two periods occurred at 08:00–11:00 when the PNCs were 35%–45% lower in 2016–2018 than 2010–2012. It should be noticed that a higher boundary-mixing layer generally occurs during afternoon rush hours and disfavors the accumulation of air pollutants, leading to only a slight increase in PNCs during this time. Overall, the nucleation-mode PNCs in 2016–2018 decreased by an average of 20% relative to that in 2010–2012. Similar results were obtained when heating and nonheating seasons were separated for comparison, for example, the nucleation-mode PNCs decreased by 25% in heating season and 13% in nonheating season in 2016–2018 relative to that in 2010–2012 (Figures S10a and S10b).

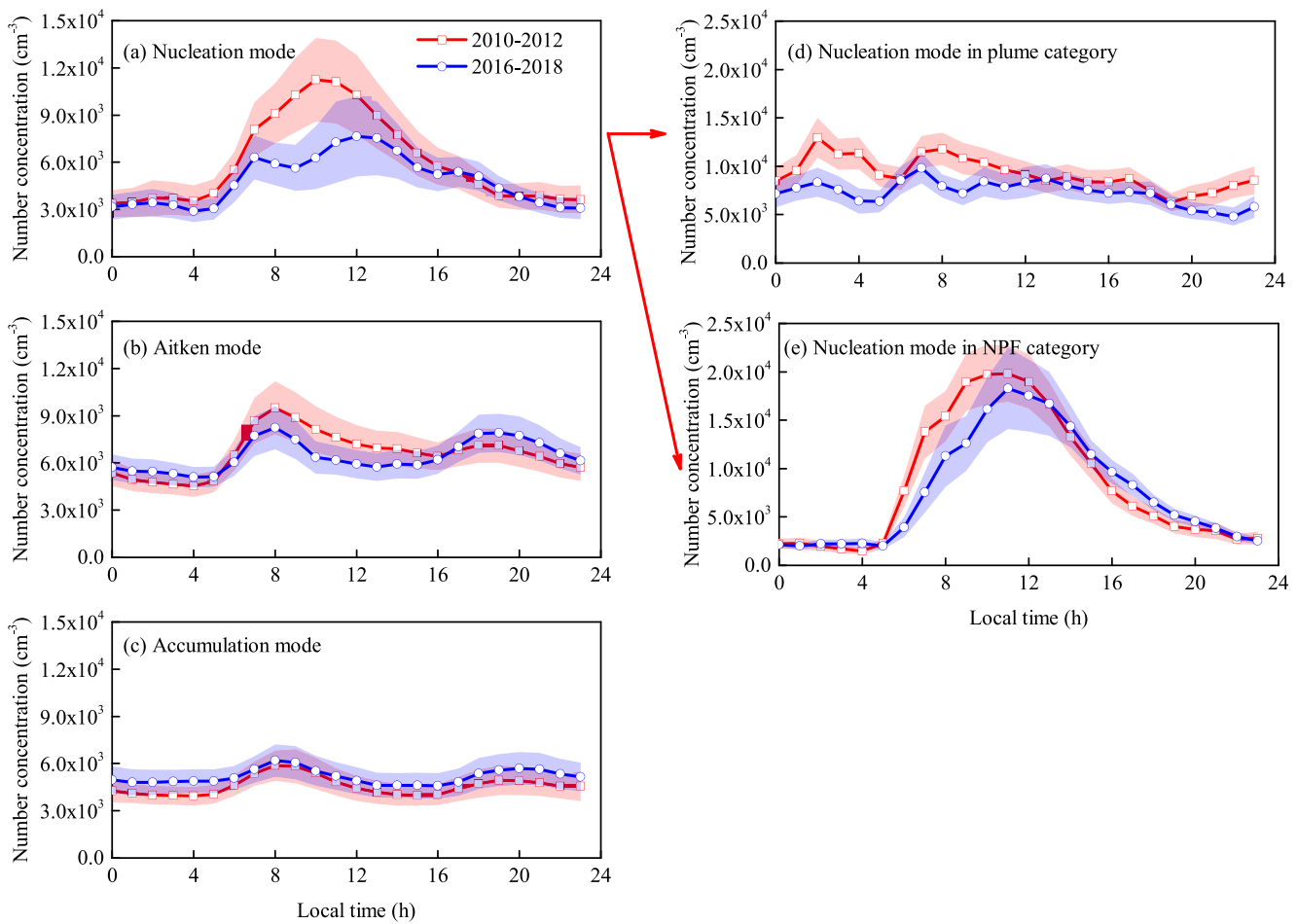


**Figure 3.** Average diurnal variations of the particle number concentrations in nucleation mode, Aitken mode, and accumulation mode during 2010–2012 (red) and 2016–2018 (blue). (d) and (e) show the nucleation-mode particles in the plume category and new particle formation category. Shaded areas represent a quarter of the standard deviations.

In each of the two periods, the diurnal variation in the Aitken-mode PNCs showed a bimodal distribution. The same was true for the accumulation-mode PNCs. The morning peak was associated with increased emissions of on-road vehicles in rush hours, but that was not the case for the night peak at 19:00–21:00 LT, which likely from combustion sources such as cooking or biomass burning. The morning peak in Aitken-mode PNCs at 08:00 LT decreased by 13% in 2016–2018 relative to the corresponding value in 2010–2012. The decrease continued from 08:00 LT through 15:00 LT with percentage values of 12%–22%. However, the PNC night peak at 19:00 LT in 2016–2018 increased by 11% relative to that in 2010–2012, and the increase extended until midnight (Figure 3b); this has yet to be explained. In heating season, the lower height of the boundary mixing layer results in the more prominent peaks than in nonheating season (Figures S10c and S10d). For the accumulation-mode particles, the hourly average PNCs in 2016–2018 were consistently larger (3%–24%) than the corresponding values in 2010–2012 (Figure 3c). However, this difference narrowed to 3%–5% at 07:00–10:00 LT, probably owing to the reduced on-road vehicle emissions in 2016–2018 relative to 2010–2012. The separate analysis of the two seasons of data showed that consistent results can be obtained only in heating seasons with higher accumulation mode PNCs (Figures S10e and S10f).

The increased accumulation-mode particles in 2016–2018 relative to 2010–2012 may have been mainly due to enhanced primary combustion emissions in 2016–2018, excluding on-road vehicle emissions. Five considerations support this possibility: (a) the difference of accumulation-mode PNCs observed in the morning rush hours was found to narrow; (b) the growth of newly formed particles in NPF events to sizes >100 nm was rarely observed (Man et al., 2015; Yu et al., 2019; Zhu et al., 2017, 2019); (c) the growth of pre-existing

Aitken-mode particles to sizes  $>100$  nm was rarely observed (i.e., the occurrence frequencies of pre-existing Aitken-mode particle growth were only 4% in 2010–2012 and 2016–2018); (d) the coagulation scavenging of  $>100$  nm particles in ambient air was negligible (X. H. Yao et al., 2005); and (e) a consistent increase in each hour occurred only in the heating season with higher PNCs (Figure S10e). Increased accumulation-mode PNCs over the last decade were also reported for a mountainous location in the North China Plain, based on wide-range particle spectrometer (WPS, Model 1000XP, MSP Corporation) measurements, implying that the increase in accumulation-mode PNCs may occur regionally. However, the increase in accumulation-mode particles is inconsistent with the decrease in  $PM_{2.5}$  mass concentrations over a large regional scale (Zhu et al., 2021).

To explore the large difference of nucleation-mode PNCs between the two periods in terms of primary and secondary contributors via NPF events, the diurnal variations in nucleation-mode PNCs were further sub-classified into plume, NPF, or background categories. We focused on the plume category and NPF category. In the plume category (Figure 3d), the nucleation-mode PNCs did not show a clear diurnal trend similar to that in Figure 3a. In 2010–2012, the elevated nucleation-mode PNCs occurred at 02:00–04:00 LT. The corresponding values in 2016–2018 decreased by 32%–43% relative to 2010–2012 over that time. The decrease was close to or larger than the decrease by 33% at 08:00–09:00 LT through the same comparison. The large decrease at 02:00–04:00 LT in 2016–2018 was presumably not caused by reduced on-road vehicle emissions. Rather, it is more likely to be due to the decreasing emissions from other combustion sources in 2016–2018.

In the NPF category (Figure 3e), a clear unimodal diurnal pattern can be identified with the maximum nucleation-mode PNCs occurring at 10:00–11:00 during the two periods. The maximum nucleation-mode PNCs in 2016–2018 was only 8% smaller than that in 2010–2012; however, the nucleation-mode PNCs at 06:00–07:00 LT in 2016–2018 were 45%–49% smaller than the corresponding values in 2010–2012. The enlarged difference of nucleation-mode PNCs at 06:00–07:00 LT in 2016–2018 relative to 2010–2012 also points to the largely reduced emissions from on-road vehicles in 2016–2018.

Overall, the nucleation-mode PNCs in 2016–2018 decreased relative to those in 2010–2012. The decrease in rush hour values was probably due to reduced emissions from on-road vehicles, whereas the decrease at midnight was probably caused by reduced emissions from other combustion sources. Reduced emissions of  $SO_2$  and  $NO_x$  from industrial combustion expectedly lowered emissions of nucleation-mode and Aitken-mode particles. NPF events probably reduced the difference in hourly average nucleation-mode PNCs in the NPF category between the two periods, largely by increasing nucleation-mode PNCs. Conversely, the accumulation-mode PNCs increased in 2016–2018 relative to those in 2010–2012, even though the accumulation-mode particles emitted from on-road vehicles probably decreased in 2016–2018.

### 3.3. Comparison of PNSDs Measured Between 2010–2012 and 2016–2018

The proportions of the three modes of PNCs in the t-PNCs in 2010–2012 and 2016–2018 are compared in Figure 4a. The overall average PNSD, as well as PNSDs in the background category, plume category, and NPF category, are shown in Figures 4b–4e, respectively. As expected, the trimodal distributions can be clearly identified in both 2010–2012 and 2016–2018. It is worth noting that the peak diameter of the accumulation-mode particles increased from 135 nm in 2010–2012 to 145 nm in 2016–2018, accompanied by an increase of accumulation-mode PNCs (Figures 4b and 4d). Similar trends can be obtained by analysis of data from heating and nonheating seasons (Figure S11). However, this increase is generally undetectable in Figures 4c and 4e where the PNSDs in the background category and NPF category are displayed. Thus, it can be reasonably inferred that the increase in the plume category in 2016–2018 was probably caused by enhanced primary emissions, and consequently led to the increase in the overall average PNSD.

In general, the PNCs of the three modes each accounted for approximately one-third of the total t-PNCs during the two periods. As mentioned, the unique increase in accumulation-mode PNCs for the plume category in 2016–2018 relative to 2010–2012 led to an increase in the corresponding proportion (Figure 4a). Conversely, a decrease in nucleation-mode PNCs in 2016–2018 caused a decrease in the corresponding proportion, leaving no change in the proportion of Aitken-mode PNCs. In the background category and NPF category, the proportions of the three PNC modes were highly consistent between the two periods. The

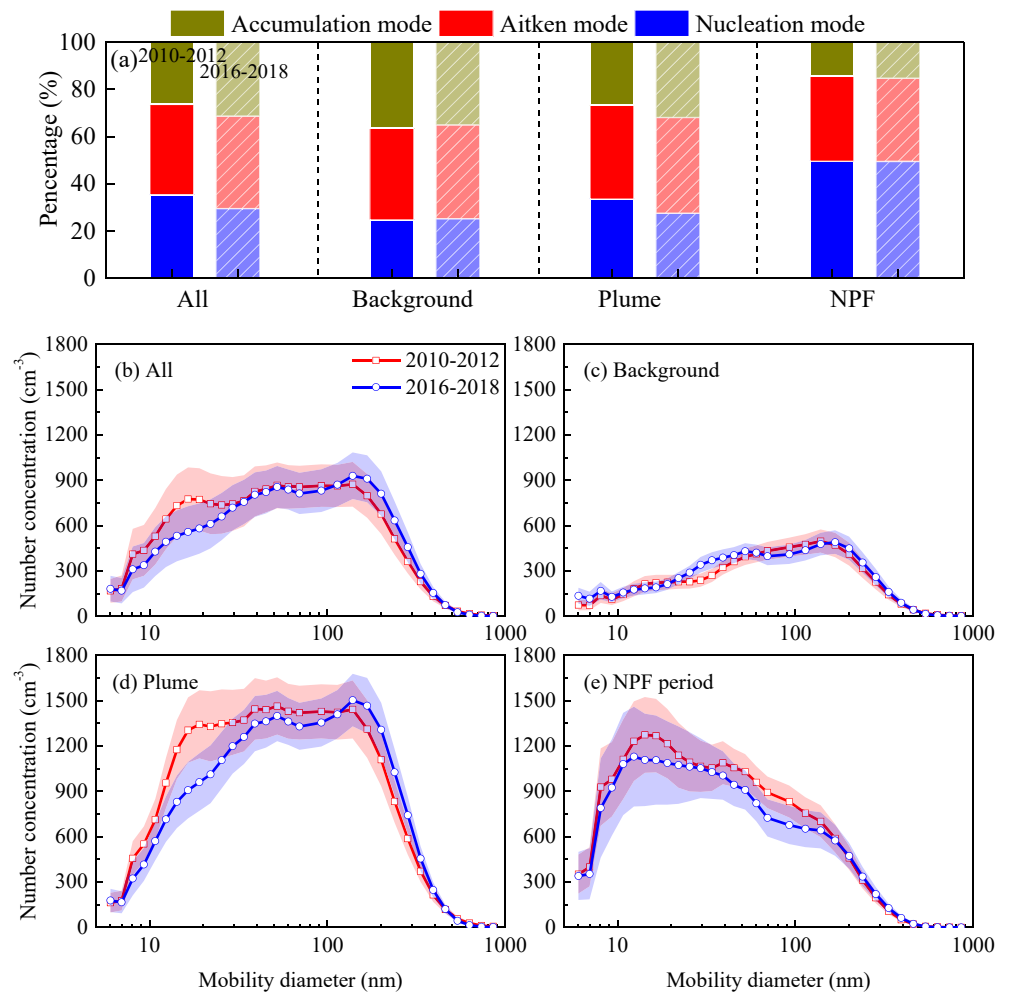


**Figure 4.** Proportions of nucleation-mode, Aitken-mode, and accumulation-mode particles in the t-PNCs (a), particle number size distributions of the overall particles (b), background category particles (c), plume category particles (d), and new particle formation category particles (e) during 2010–2012 (red) and 2016–2018 (blue). Shaded areas represent a quarter of the standard deviations.

possible impacts of the changed PNSDs on the climate in terms of the annual variations in cloud properties over Qingdao are further discussed in Section 4.2.

### 3.4. Comparison of Observed NPF Events Between 2010–2012 and 2016–2018

NPF events can be identified on 96 of the 281 sampling days in 2010–2012 versus 85 of the 343 sampling days in 2016–2018, with corresponding occurrence frequencies of 34% and 25%, respectively (Figure 5a). The NPF events were classified into three groups according to their potential climate impacts. In the group 1 events (Figure 5b), the  $D_{pgmax}$  of grown new particles was <50 nm, and these were too small to be activated as CCN. In the group 2 events (Figure 5c), the  $D_{pgmax}$  of grown new particles exceeded 50 nm, and these may have been activated as CCN at different ambient super-saturation levels. In the group 3 events, the final  $D_{pgmax}$  of NPF events was unable to be determined in the presence of the invading plumes. No further analysis of group 3 events are presented in this study.

In 2010–2012, group 1 events occurred on 20% of the 281 sampling days and group 2 events occurred on 10% of the days. In 2016–2018, the occurrence frequencies of groups 1 and 2 events decreased to 18% and 4%, respectively. The decrease in NPF frequencies also occurred in heating and nonheating seasons (Figure 5a).

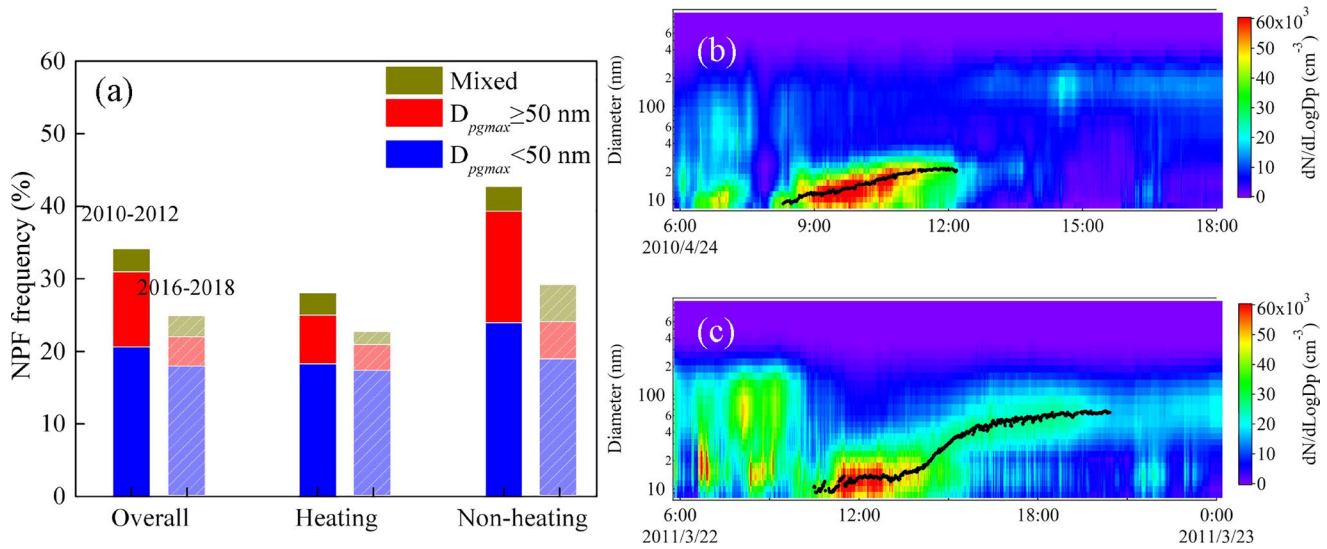


**Figure 5.** Occurrence frequencies of new particle formation (NPF) events in 2010–2012 and 2016–2018 (a), and examples of NPF events in two groups: group 1 on April 24, 2010 in which  $D_{pgmax} < 50$  nm (b); group 2 on March 22, 2011 in which  $D_{pgmax} \geq 50$  nm (c).

For example, in nonheating seasons, the occurrence frequency of group 2 events exhibited the largest decrease, from 15% in 2010–2012 to 5% in 2016–2018.

Four metrics, that is, the apparent FR, NMINP, GR, and  $D_{pgmax}$ , were used to characterize the NPF events (Figure 6). There was no significant difference of apparent FR, NMINP, and GR between 2010–2012 and 2016–2018 with  $p > 0.05$ . However, the  $D_{pgmax}$  values in 2016–2018 were significantly smaller than those in 2010–2012 with  $p < 0.05$ . A large difference of air pollutant concentrations is generally observed between

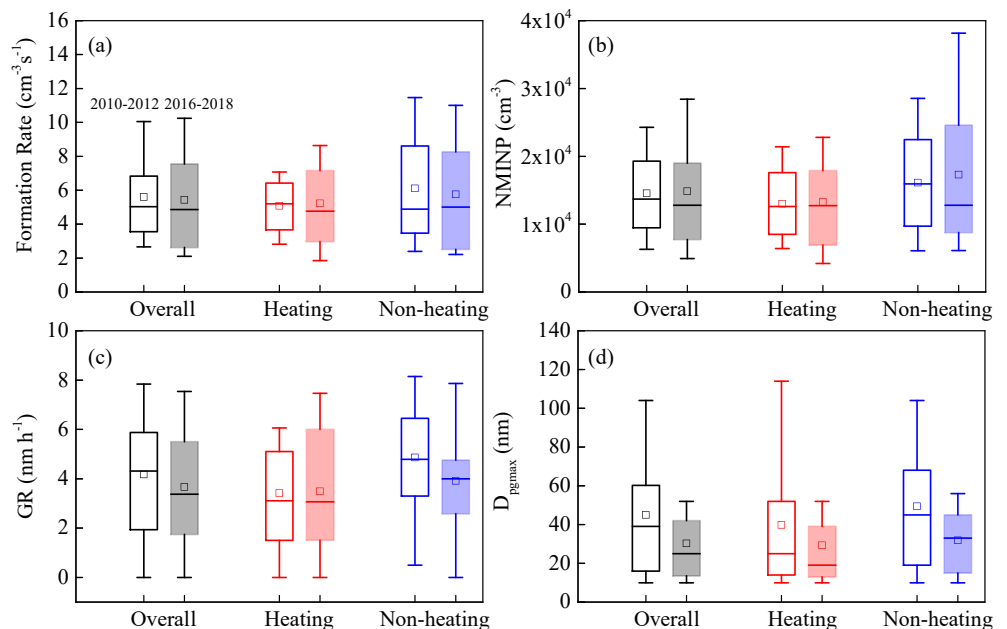


**Figure 6.** Box plots of apparent new particle formation rate (a), net maximum increase in the nucleation-mode particle number concentration (NMINP, b), new particle growth rate (GR, c), and maximum geometric median diameter of new particles ( $D_{pgmax}$ , d). The left black column in each season represents 2010–2012 and the right solid column in each season represents 2016–2018. The upper and lower boundaries of the box indicate the 75th and the 25th percentiles, respectively, the line within the box marks the median, and the whiskers above and below the box indicate the 90th and tenth percentiles. The squares represent the mean values.

the heating season and the nonheating season (Xiao et al., 2015). In addition, a large difference in biogenic VOC concentrations was, as expected, observed between the heating and nonheating seasons because of temperature effects, although no direct measurements were available. The four metrics in 2010–2012 and 2016–2018 are compared separately in the heating and nonheating seasons and the same results are obtained. The details are presented below.

For the apparent FRs, the overall average values were nearly the same, that is,  $5.6 \text{ cm}^{-3} \text{ s}^{-1}$  in 2010–2012 versus  $5.4 \text{ cm}^{-3} \text{ s}^{-1}$  in 2016–2018 (Figure 6a). The average values in the heating seasons were  $5.1 \text{ cm}^{-3} \text{ s}^{-1}$  in 2010–2012 versus  $5.2 \text{ cm}^{-3} \text{ s}^{-1}$  in 2016–2018, whereas the two values were  $6.1 \text{ cm}^{-3} \text{ s}^{-1}$  versus  $5.8 \text{ cm}^{-3} \text{ s}^{-1}$  in the nonheating seasons. Note that there were large variations in the apparent FR in each of the two periods. For example, the 10th and 90th percentiles of the apparent FR were  $2.7 \text{ cm}^{-3} \text{ s}^{-1}$  and  $10.0 \text{ cm}^{-3} \text{ s}^{-1}$ , respectively, in 2010–2012, and  $2.1 \text{ cm}^{-3} \text{ s}^{-1}$  and  $10.2 \text{ cm}^{-3} \text{ s}^{-1}$  in 2016–2018.

For NMINP, the overall averages in 2010–2012 and 2016–2018 were the same at  $1.5 \times 10^4 \text{ cm}^{-3}$ . When the heating seasons were examined alone, the average values decreased to  $1.3 \times 10^4 \text{ cm}^{-3}$  in each of the two periods. In the nonheating seasons, the average values increased to  $1.6 \times 10^4 \text{ cm}^{-3}$  in 2010–2012 and  $1.7 \times 10^4 \text{ cm}^{-3}$  in 2016–2018.

For GR, the overall average values were  $4.2 \text{ nm h}^{-1}$  in 2010–2012 and  $3.7 \text{ nm h}^{-1}$  in 2016–2018. In the nonheating seasons, the two average values were  $4.9 \text{ nm h}^{-1}$  in 2010–2012 versus  $3.9 \text{ nm h}^{-1}$  in 2016–2018. In the heating seasons, the two average values were almost the same, that is,  $3.4 \text{ nm h}^{-1}$  in 2010–2012 versus  $3.5 \text{ nm h}^{-1}$  in 2016–2018.

For  $D_{\text{pgmax}}$ , the overall averages were 45 nm in 2010–2012 versus 30 nm in 2016–2018. Lower values of  $D_{\text{pgmax}}$  in 2016–2018 relative to 2010–2012 were also obtained in both the heating (29 vs. 40 nm) and nonheating seasons (32 vs. 49 nm).

In summary, the averages of apparent FR and NMINP were almost the same in 2010–2012 and in 2016–2018. Although no significant decrease in GR was occurred in 2016–2018 relative to 2010–2012, the decrease in  $D_{\text{pgmax}}$  was significant and large in 2016–2018, which lowered the probability of new grown particles being activated as CCN. The reasons for the difference in this NPF characteristic between the two time periods are discussed in Section 4.1.

## 4. Discussion

### 4.1. Factors Affecting the Occurrence Frequency and Four Metrics of the NPF Events

Sulfuric acid formed by oxidation of ambient  $\text{SO}_2$  is considered a key precursor species for ambient nucleation in the continental atmosphere. A large decrease in  $\text{SO}_2$  concentrations has been observed across China in the past decade (Krotkov et al., 2016; X. Li et al., 2020; T. Wang et al., 2018). Between 2010–2012 and 2016–2018, the ambient concentration of  $\text{SO}_2$  decreased by ~60%, and the decreases in the percentage were almost identical in heating and nonheating seasons (Figure S12a). The decrease in ambient  $\text{SO}_2$  concentrations may be the primary factor lowering the occurrence frequency of NPF events. The decreasing occurrence frequency with decreasing  $\text{SO}_2$  concentration has been previously reported in urban areas, such as Pittsburgh (U.S.A.), Rochester (U.S.A.), and Melpitz (Germany) (Hamed et al., 2010; Saha et al., 2018; Y. Wang et al., 2011; Z. B. Wang et al., 2017). In this study, there were no significant changes in the apparent FR and NMINP values between the two periods. As shown in Figure S13, a weak correlation was obtained between FR and  $\text{SO}_2$  concentration ( $r = 0.44$ ,  $p < 0.05$ ), while no significant correlation can be obtained between  $\text{SO}_2$  concentration and NMINP ( $p > 0.05$ ). Our results imply that in addition to the concentrations of  $\text{SO}_2$ , the apparent FR and NMINP values were also affected by multiple factors, such as biogenic precursors, amines, CS value, oxidants, and meteorological conditions (Chu et al., 2019; S. H. Lee et al., 2019; Tröstl et al., 2016).

No  $\text{PM}_{2.5}$  data were available before 2012, but the average  $\text{PM}_{2.5}$  concentration in Qingdao was reduced by 41% in 2016–2018 relative to 2013 because of the tightened control measures on air pollutant emissions since 2013. However, no significant decrease in CS was present in 2016–2018 relative to 2010–2012 (Figure 7a). For example, the average CS was  $4.0 \times 10^{-2} \text{ s}^{-1}$  in 2010–2012 and  $3.8 \times 10^{-2} \text{ s}^{-1}$  in 2016–2018. The same trend was obtained when the CS in the heating seasons was considered separately. The CS prior to the

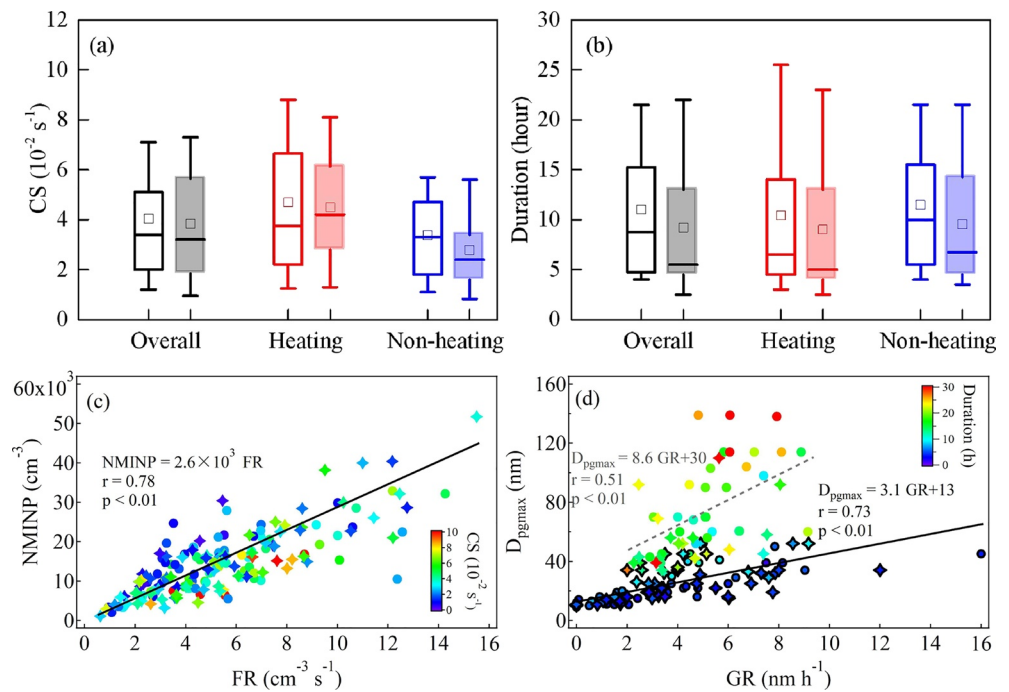


**Figure 7.** Box plots of condensation sink (CS, a) and new particle formation (NPF) event duration (b), the scatter plots of apparent formation rate (FR) and new particle formation (NPF) color-coded with CS (c), growth rate (GR) and the maximum size of the geometric median diameter of the new particles ( $D_{\text{pgmax}}$ ) color-coded with NPF duration (d). In (a) and (b), the left column in each season represents 2010–2012 and the right columns represent 2016–2018. The upper and lower boundaries of the box indicate the 75th and the 25th percentiles, respectively, the line within the box marks the median, and the whiskers above and below the box indicate the 90th and tenth percentiles. The squares represent the mean values. In (c) and (d), the circles and stars represent the data in 2010–2012 and 2016–2018, respectively. Markers outlined in black in (d) represent NPF events with one-stage growth. The black and gray lines and equations in (d) were fitted by one-stage and two (or multi)-stage growth NPF events, respectively.

NPF events was determined mainly by the accumulation-mode particles, which contribute most to the aerosol surface area (Gong et al., 2010; Kumar et al., 2014; Zhu et al., 2021). The particle number concentration in 2016–2018 (100–300 nm) was slightly greater than that in 2010–2012 (Figure 4), and may have resulted in the almost unchanged CS, although the  $\text{PM}_{2.5}$  concentration also decreased markedly. A case-by-case analysis of the observed apparent FRs, NMNIPs and CSs revealed that larger CS values were always associated with lower NMNIP/FR ratios (Figure 7c). This is expected, given the coagulation-loss term used in the calculation of FR (see (equation 1) in Supporting Information S1).

Figure 7c shows a strong linear correlation between the apparent FR and NMNIP ( $r = 0.78$ ,  $p < 0.01$ ). The fitted equation is highly consistent with our previous results derived from urban, marine, and mountain atmospheres (L. Ma et al., 2021; Man et al., 2015; Zhu et al., 2017, 2019, 2021). As mentioned, sulfuric acid formed by the oxidization of  $\text{SO}_2$  is commonly considered as the key precursor for ambient nucleation in the continental atmosphere. Previous studies have shown that the concentration of gaseous sulfuric acid must be greater than  $10^5$  molecules  $\text{cm}^{-3}$  for NPF events, while the reported daytime sulfuric acid concentrations are mostly in the range of  $10^6$ – $10^7$  molecules  $\text{cm}^{-3}$  in China and are thus theoretically sufficient for NPF (Erupe et al., 2010; S. H. Lee et al., 2019; X. Li et al., 2020; McMurry et al., 2005; Nieminen et al., 2009; Zhu et al., 2021). We proposed that sulfuric acid vapor was sufficient for nucleation and that the NPF intensity was probably determined by the abundance of organic vapors available for participating in nucleation. According to the literature, the HOMs oxidized from VOCs and amines can participate in and enhance nucleation in the continental troposphere (Ehn et al., 2014; S. H. Lee et al., 2019; Tröstl et al., 2016; L. Yao et al., 2018; R. Zhang et al., 2012). Increased FR under reduced  $\text{SO}_2$  conditions has been reported in Hyytiälä Forest (Finland) and at Mt. Tai (China), which were attributed to the increased biogenic VOC emissions (Nieminen et al., 2014; Zhu et al., 2021). In the region of the sampling site, the estimated emissions of biogenic VOC increased by  $\sim 10\%$  between the two periods, mainly because of the increase in forested area

(Figure S2a, W. H. Chen et al., 2018; H. Wang et al., 2021; Wang, Feng, et al., 2020; X. D. Zhang et al., 2016). However, no long-term measurements of VOCs and HOMs were made in this study. H. Wang et al. (2021) also reported that the satellite-determined formaldehyde column density showed statistically significant positive correlation coefficients over regions with high fractions of vegetative cover. The density values during the heating and nonheating seasons increased by  $\sim 18\%$  and  $5\%$  in 2016–2018 relative to 2010–2012 (Figure S12b), suggesting that there had been an increase in the concentration of oxidized VOCs. Moreover, the measured concentrations of atmospheric  $\text{NH}_3$  in Qingdao, based on the data from the Nationwide Nitrogen Deposition Monitoring Network, also exhibited an  $\sim 59\%$  increase in 2015 relative to 2011–2012 (Figure S12c, no data are available for later than 2016). Thus, the effect of the large decrease in  $\text{SO}_2$  concentrations may have been substantially negated, leading to the invariant FR and NMINP values observed between the two periods in Qingdao.

Differing from the apparent FR and NMINP,  $D_{\text{pgmax}}$  showed a significant decrease in 2016–2018 compared with 2010–2012. Theoretically, the  $D_{\text{pgmax}}$  should be linearly correlated with the product of GR and NPF duration when the newly formed particles undergo typical banana-shaped one-stage growth. However, two-stage growth or multi-stage growth (see example in Figure S14) more frequently occur in various atmospheres, whereby the growth of newly formed particles stops for a few hours, possibly because the condensation vapors are inadequate to support growth. The growth of new particles restarts when condensable vapor concentrations are higher than the required values, and the restarted process is mainly determined by semi-volatile compounds (L. Ma et al., 2021; Man et al., 2015; Zhu et al., 2014, 2019). The correlation between GR and  $D_{\text{pgmax}}$  at varying NPF durations is shown in Figure 7d for all of the NPF events observed during the two periods. Considering the NPF events where only one-stage growth occurred (symbols outlined in black), the GR and  $D_{\text{pgmax}}$  values showed a strong linear relationship ( $r = 0.73$  and  $p < 0.01$ ). Considering the two (or multi)-stage growth events alone, the GR (average value of each growth stage) showed a weak correlation with  $D_{\text{pgmax}}$  ( $r = 0.51$  and  $p < 0.01$ ). The  $D_{\text{pgmax}}$  values in the two (or multi)-stage growth events were significantly larger than those in the one-stage growth (Figure 7d). The same is true for GR and NPF duration. The two (or multi)-stage growth NPF events occurred on 29 days in 2010–2012 and 17 days in 2016–2018. The decreased occurrence frequency of two (or multi)-stage growth NPF events led to the smaller  $D_{\text{pgmax}}$  in 2016–2018. In addition, the shorter NPF duration in 2016–2018 implies that the events occurred over a smaller spatial scale. Note that the  $D_{\text{pgmax}}$  of group 1 events did not exhibit a statistically significant change in 2016–2018 ( $23 \pm 12$  nm) relative to that in 2010–2012 ( $25 \pm 13$  nm), as the  $p$  value was  $> 0.05$ .

The decreased  $\text{SO}_2$  concentration may directly affect the concentration of sulfuric acid vapor and reduce its contribution to the growth of newly formed particles. However, no significant correlation can be obtained between  $\text{SO}_2$  concentration and GR,  $D_{\text{pgmax}}$  ( $p > 0.05$ , Figures S13c and S13d). On the other hand, the reduced amount of sulfuric acid condensed on newly formed particles may also reduce the aerosol acidity, subsequently affecting the acid-enhanced uptake of semi-volatile organic species (Ding et al., 2011; Stangl et al., 2019). Ammonium nitrate has also been reported to promote the second-stage growth of new particles at nighttime (X. H. Liu et al., 2014; L. Ma et al., 2021; Man et al., 2015; Zhu et al., 2014). In our campaign-based studies, that is, 2012/2013 winter campaign (December 6, 2012–January 24, 2013) and 2017/2018 winter campaign (December 14, 2017–January 6, 2018), the mass concentration of sulphate in  $\text{PM}_{2.5}$  largely decreased from  $17 \pm 11 \mu\text{g m}^{-3}$  to  $4.4 \pm 4.5 \mu\text{g m}^{-3}$ . Meanwhile, the mass concentration of nitrate in  $\text{PM}_{2.5}$  also decreased from  $11.5 \pm 7.9 \mu\text{g m}^{-3}$  in the 2012/2013 winter campaign to  $8.8 \pm 8.5 \mu\text{g m}^{-3}$  in the 2017/2018 winter campaign. Unfortunately, we did not measure the precursor vapors and have no data on the semi-VOCs throughout the observation periods.

#### 4.2. Elucidating the Complex Relationship Between Atmospheric Particles and Cloud Properties

The satellite-based AOD, cloud fraction (CF), cloud optical thickness (COT), cloud effective radius (CER), and cloud water path in liquid phase (CWP) were analyzed during 2010–2019 to better understand the possible climate impacts of the changed PNSD between the two periods. The monthly mean of the AOD, COT, CF, CER, and CWP values from the moderate-resolution imaging spectroradiometer (MODIS) level-3 (L3) cloud product ([https://ladsweb.modaps.eosdis.nasa.gov/search/order/1/MOD08\\_M3](https://ladsweb.modaps.eosdis.nasa.gov/search/order/1/MOD08_M3)) over Qingdao were used to estimate the annual and seasonal averages in each year (Figure 8). AOD and CF showed a

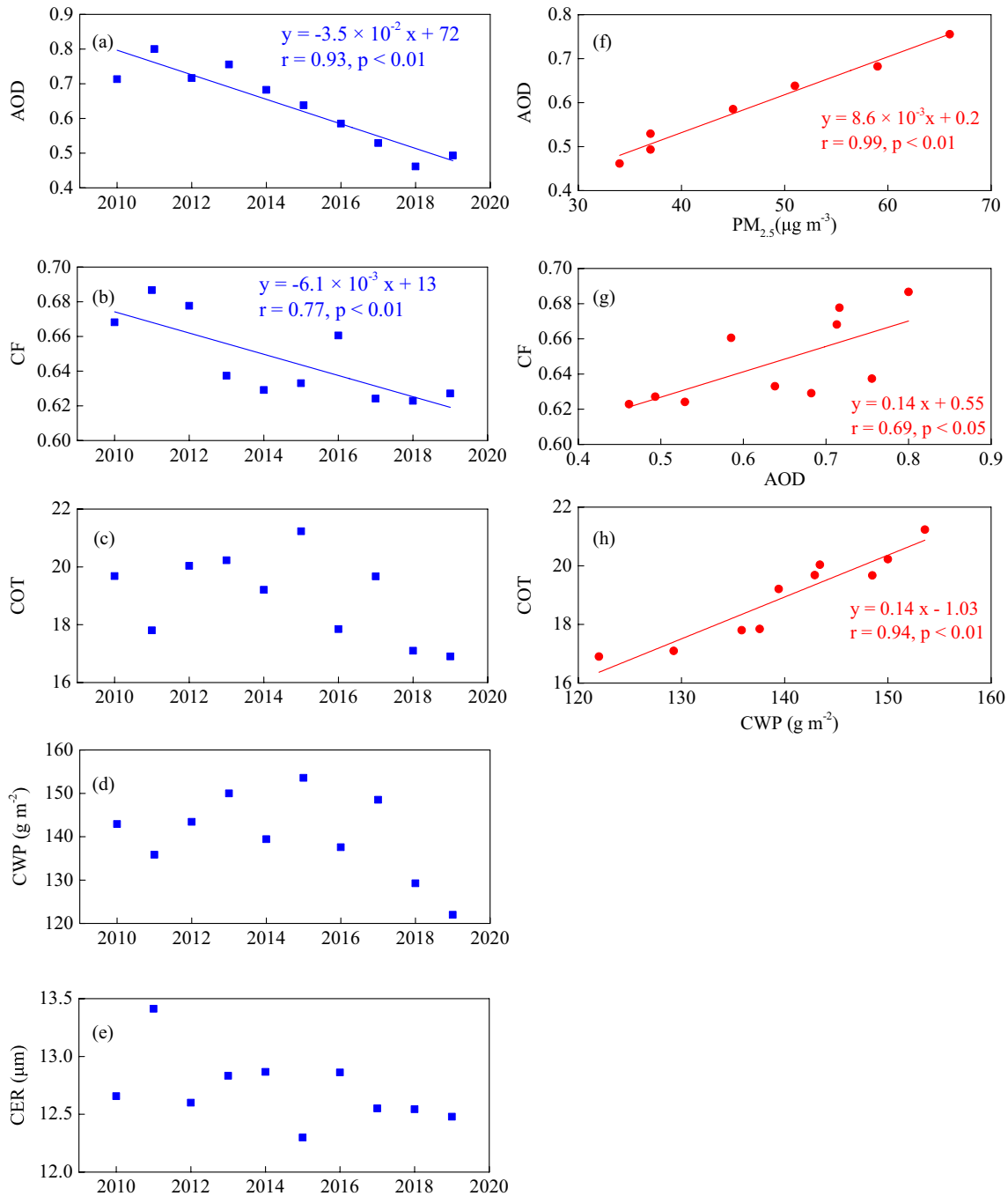


**Figure 8.** Time series of satellite retrieved aerosol optical depth (AOD, a), cloud fraction (CF, b), cloud optical thickness (COT, c), cloud water path (CWP, d), and cloud effective radius (CER, e) from 2010 to 2019, and the relationship between observed  $\text{PM}_{2.5}$  mass concentration and satellite retrieved AOD (f), AOD and CF (g), CWP and COT (h) in Qingdao. (satellite data obtained from [https://ladsweb.modaps.eosdis.nasa.gov/search/order/1/MOD08\\_M3](https://ladsweb.modaps.eosdis.nasa.gov/search/order/1/MOD08_M3)).

significant decreasing trend ( $p < 0.01$ ) since 2013, according to regression analysis and the Mann–Kendall test. The overall  $\sim 40\%$  decrease in AOD is consistent with the nearly identical percentage decrease in mass concentrations of  $\text{PM}_{2.5}$  observed at the ground level. However, the CF decreased by only  $\sim 6\%$  from 2010 to 2019. The decrease in aerosol loadings may have caused a decrease in CF to some extent, on the basis of the significant correlation between AOD and CF ( $r = 0.69$ ,  $p < 0.05$ , Figure 8g). Note that no significant correlation exists between CF and CWP and the downward trend in CF was unlikely to have been driven by CWP. In addition, the regression analysis showed no significant trend in COT, whereas a stable trend was

revealed by the Mann–Kendall test. COT was strongly correlated with CWP ( $r = 0.94$ ,  $p < 0.01$ , Figure 8h), which suggests a negligible influence of the changed aerosol loadings on COT. The regression analysis also showed no significant trend in CER, whereas the Mann–Kendall test showed a probable decreasing trend in CER from 2013 to 2019 with  $p = 0.054$ .

In this study, the observed accumulation-mode PNCs in 2016–2018 increased by an average of 11% relative to those in 2010–2012, probably due to enhanced primary emissions. The increased accumulation-mode PNCs may not have led to an increase in CCN, because of the low cloud activities of primary aerosols from combustion sources (Zhu et al., 2019; Gao et al., 2020; Figure S15). However, the decreasing extent of CCN in the atmosphere may be substantially smaller than that of AOD, leading to a smaller percentage decrease in CF, no significant trend in CER, and a negligible detectable influence on COT.

## 5. Conclusions

PNCs, PNSDs, and NPF events were analyzed to evaluate the possible influence of reduced anthropogenic emissions on the concentrations of primary and secondary particles between 2010–2012 and 2016–2018 in a semi-urban area in Qingdao, a coastal city in northern China. The PNCs slightly decreased by an average of 5% in 2016–2018 relative to 2010–2012, despite a large decrease (>40%) in the  $PM_{2.5}$  mass concentration. The nucleation-mode PNCs decreased substantially by an average of 20%. The decrease in nucleation-mode PNCs between rush hour and midnight was mainly attributable to the decrease in primary emissions in this period, such as emissions from on-road vehicles and other combustion sources, while the decrease in nucleation-mode PNCs at 08:00–12:00 may have been due to the 9% decrease in NPF occurrence frequency. In contrast, the accumulation-mode PNCs increased by an average of 11% with increasing median diameter of accumulation-mode particles. When the heating and nonheating seasons were separately analyzed, the nucleation-mode PNCs decreased by 25% in heating season and 14% in nonheating season, while the accumulation-mode PNCs increased by 11% in heating season with a negligible change in nonheating season.

Considering that the concentrations of  $SO_2$  strongly decreased by ~60% between 2010–2012 and 2016–2018 with similar percentages in heating and nonheating seasons, NPF events during the two periods were compared in terms of occurrence frequency, apparent FR, NMINP, GR,  $D_{pgmax}$  and their correlations with  $SO_2$ . The occurrence frequencies of NPF events decreased from 34% in 2010–2012 to 25% in 2016–2018. However, no significant changes occurred in NPF intensity, that is, apparent FR and NMINP, in 2016–2018 relative to 2010–2012. This probably due to other factors such as increased atmospheric VOCs and  $NH_3$  offsetting the reduction in  $SO_2$ , resulting in the invariant FR and NMINP values. The maximum sizes of grown new particles decreased by 50% in 2016–2018, which is mainly attributed to the fewer precursors were not sufficient to proceed the two (or multi)-stage growth of new particles. The decrease in concentrations of particulate sulphate and nitrate in 2016–2018 relative to 2010–2012 seems to have restricted the growth of newly formed particles to some extent. Overall, it can be concluded that the increased accumulation-mode PNCs in 2016–2018 were unlikely to have been caused by the NPF events that occurred in that period. Since no emission inventory of PNCs in China is available, the weakness restricts the study to apportion the observed overall changes between two periods to each secondary or primary source.

The AOD and  $PM_{2.5}$  mass concentrations largely decreased by ~40% after 2013. Although a downward trend in CF has indeed existed since 2010, the overall decreasing percentage was only 6%. Moreover, no influence of decreasing aerosol optical or mass loadings on COT can be detected, while there is a probable decreasing trend in CER. The increased accumulation-mode PNCs in 2016–2018 relative to 2010–2012, suggest that decreased concentration of CCN in 2016–2018 may be substantially smaller than the value of AOD and the  $PM_{2.5}$  mass concentrations. Continuous observations and modeling studies are required to more fully understand the long-term trends of different PNC modes and their health and climate impacts.

## Data Availability Statement

Data associated with this paper are accessible at <https://data.mendeley.com/datasets/jx8y92fdfx/draft?a=8720245d-159b-4718-a165-844271675939>.

### Acknowledgments

This work was funded by the National Natural Science Foundation of China (42075104, 41922051, 41776086, 42061160478), China Postdoctoral Science Foundation (2019M662363), and the Jiangsu Collaborative Innovation Center for Climate Change.

### References

- Asmi, E., Kivekäs, N., Kerminen, V. M., Komppula, M., Hyvärinen, A. P., Hatakka, J., et al. (2011). Secondary new particle formation in Northern Finland Pallas site between the years 2000 and 2010. *Atmospheric Chemistry and Physics*, *11*(24), 12959–12972. <https://doi.org/10.5194/acp-11-12959-2011>
- Bianchi, F., Trostl, J., Junninen, H., Frege, C., Henne, S., Hoyle, C. R., et al. (2016). New particle formation in the free troposphere: A question of chemistry and timing. *Science*, *352*(6289), 1109–1112. <https://doi.org/10.1126/science.aad5456>
- Charlson, R. J., Schwartz, S. E., Hales, J. M., Cess, R. D., Coakley, J. A., Hansen, J. E., & Hofmann, D. J. (1992). Climate forcing by anthropogenic aerosols. *Science*, *255*(5043), 423–430. <https://doi.org/10.1126/science.255.5043.423>
- Chen, C., Park, T., Wang, X. H., Piao, S. L., Xu, B. D., Chaturvedi, R. K., et al. (2019). China and India lead in greening of the world through land-use management. *Nature Sustainability*, *2*(2), 122–129. <https://doi.org/10.1038/s41893-019-0220-7>
- Chen, W. H., Guenther, A. B., Wang, X. M., Chen, Y. H., Gu, D. S., Chang, M., et al. (2018). Regional to global biogenic isoprene emission responses to changes in vegetation from 2000 to 2015. *Journal of Geophysical Research: Atmospheres*, *123*, 3757–3771. <https://doi.org/10.1002/2017JD027934>
- Chu, B., Kerminen, V. M., Bianchi, F., Yan, C., Petäjä, T., & Kulmala, M. (2019). Atmospheric new particle formation in China. *Atmospheric Chemistry and Physics*, *19*, 115–138. <https://doi.org/10.5194/acp-19-115-2019>
- Dal Maso, M., Kulmala, M., Riiipinen, I., Wagner, R., Hussein, T., Aalto, P. P., et al. (2005). Formation and growth of fresh atmospheric aerosols: Eight years of aerosol size distribution data from SMEAR II, Hyytiälä, Finland. *Boreal Environment Research*, *10*(5), 323–336.
- Ding, X., Wang, X., & Zheng, M. (2011). The influence of temperature and aerosol acidity on biogenic secondary organic aerosol tracers: Observations at a rural site in the central Pearl River Delta region, South China. *Atmospheric Environment*, *45*, 1303–1311. <https://doi.org/10.1016/j.atmosenv.2010.11.057>
- Dusek, U., Frank, G. P., Hildebrandt, L., Curtius, J., Schneider, J., Walter, S., et al. (2006). Size matters more than chemistry for cloud-nucleating ability of aerosol particles. *Science*, *312*(5778), 1375–1378. <https://doi.org/10.1126/science.1125261>
- Ehn, M., Thornton, J. A., Kleist, E., Sipila, M., Junninen, H., & Pullinen, I., et al. (2014). A large source of low volatility secondary organic aerosol. *Nature*, *506*(7489), 476–479. <https://doi.org/10.1038/nature13032>
- Erupe, M. E., Benson, D. R., Li, J., Young, L. H., Verheggen, B., Al-Refai, M., et al. (2010). Correlation of aerosol nucleation rate with sulfuric acid and ammonia in Kent, Ohio: An atmospheric observation. *Journal of Geophysical Research*, *115*, D23216. <https://doi.org/10.1029/2010JD013942>
- Gao, Y., Zhang, D., Wang, J., Gao, H., & Yao, X. (2020). Variations in  $N_{cn}$  and  $N_{ccn}$  over marginal seas in China related to marine traffic emissions, new particle formation and aerosol aging. *Atmospheric Chemistry and Physics*, *20*(16), 9665–9677. <https://doi.org/10.5194/acp-20-9665-2020>
- Gerling, L., Wiedensohler, A., & Weber, S. (2021). Statistical modelling of spatial and temporal variation in urban particle number size distribution at traffic and background sites. *Atmospheric Environment*, *224*, 117925. <https://doi.org/10.1016/j.atmosenv.2020.117925>
- Gong, Y., Hu, M., Cheng, Y., Su, H., Yue, D., Liu, F., et al. (2010). Competition of coagulation sink and source rate: New particle formation in the Pearl River Delta of China. *Atmospheric Environment*, *44*(27), 3278–3285. <https://doi.org/10.1016/j.atmosenv.2010.05.049>
- Hamed, A., Birmili, W., Joutsensaari, J., Mikkonen, S., Asmi, A., Wehner, B., et al. (2010). Changes in the production rate of secondary aerosol particles in Central Europe in view of decreasing SO<sub>2</sub> emissions between 1996 and 2006. *Atmospheric Chemistry and Physics*, *10*(3), 1071–1091. <https://doi.org/10.5194/acp-10-1071-2010>
- Harrison, R. M., Beddows, D. C. S., & Dall'Osto, M. (2011). PMF analysis of wide-range particle size spectra collected on a major highway. *Environmental Science & Technology*, *45*(13), 5522–5528. <https://doi.org/10.1021/es2006622>
- Heal, M. R., Kumar, P., & Harrison, R. M. (2012). Particles, air quality, policy and health. *Chemical Society Reviews*, *41*(19), 6606–6630. <https://doi.org/10.1039/c2cs35076a>
- Hoppel, W. A., Frick, G. M., & Larson, R. E. (1986). Effect of nonprecipitating clouds on the aerosol size distribution in the marine boundary layer. *Geophysical Research Letters*, *13*, 125–128. <https://doi.org/10.1029/gl013i002p00125>
- Huang, X., Wang, C., Peng, J., He, L., Cao, L., Zhu, Q., et al. (2017). Characterization of particle number size distribution and new particle formation in Southern China. *Journal of Environmental Science*, *51*, 342–351. <https://doi.org/10.1016/j.jes.2016.05.039>
- IPCC. (2013). The physical science basis. In T. F. Stocker, D. Qin, G. K. Plattner, M. Tignor, S. K. Allen, J. Boschung, et al. (Eds.), *Contribution of working Group I to the Fifth assessment report of the intergovernmental panel on climate change*. Cambridge, United Kingdom and New York, NY, USA: Cambridge University Press. <https://www.ipcc.ch/report/ar5/wg1/>
- Kerminen, V. M., Chen, X., Vakkari, V., Petäjä, T., Kulmala, M., & Bianchi, F. (2018). Atmospheric new particle formation and growth: Review of field observations. *Boreal Environment Research*, *13*, 103003. <https://doi.org/10.1088/1748-9326/Aadf3c>
- Kivekäs, N., Sun, J., Zhan, M., Kerminen, V.-M., Hyvärinen, A., Komppula, M., et al. (2009). Long term particle size distribution measurements at Mount Waliguan, a high-altitude site in inland China. *Atmospheric Chemistry and Physics*, *9*, 5461–5474. <https://doi.org/10.5194/acp-9-5461-2009>
- Krotkov, N. A., McLinden, C. A., Li, C., Lamsal, L. N., Celarier, E. A., Marchenko, S. V., et al. (2016). Aura OMI observations of regional SO<sub>2</sub> and NO<sub>2</sub> pollution changes from 2005 to 2015. *Atmospheric Chemistry and Physics*, *16*(7), 4605–4629. <https://doi.org/10.5194/acp-16-4605-2016>
- Kulmala, M., Dada, L., Dällenbach, K., Yan, C., Stolzenburg, D., Kontkanen, J., et al. (2021). Is reducing new particle formation a plausible solution to mitigate particulate air pollution in Beijing and other Chinese megacities? *Faraday Discussions*, *226*, 334–347. <https://doi.org/10.1039/d0fd00078g>
- Kulmala, M., & Kerminen, V. M. (2008). On the formation and growth of atmospheric nanoparticles. *Atmospheric Research*, *90*, 132–150. <https://doi.org/10.1016/j.atmosres.2008.01.005>
- Kulmala, M., Kontkanen, J., Junninen, H., Lehtipalo, K., Manninen, H. E., Nieminen, T., et al. (2013). Direct observations of atmospheric aerosol nucleation. *Science*, *339*(6122), 943–946. <https://doi.org/10.1126/science.1227385>
- Kulmala, M., Petäjä, T., Kerminen, V. M., Kujansuu, J., Ruuskanen, T., Ding, A. J., et al. (2016). On secondary new particle formation in China. *Frontiers of Environmental Science & Engineering*, *10*, 08. <https://doi.org/10.1007/s11783-016-0850-1>
- Kulmala, M., Petäjä, T., Nieminen, T., Sipilä, M., Manninen, H. E., Lehtipalo, K., et al. (2012). Measurement of the nucleation of atmospheric aerosol particles. *Nature Protocols*, *7*(9), 1651–1667. <https://doi.org/10.1038/nprot.2012.091>
- Kumar, P., Morawska, L., Birmili, W., Paasonen, P., Hu, M., Kulmala, M., et al. (2014). Ultrafine particles in cities. *Environment International*, *66*, 1–10. <https://doi.org/10.1016/j.envint.2014.01.013>

- Kumar, P., Robins, A., Vardoulakis, S., & Britter, R. (2010). A review of the characteristics of nanoparticles in the urban atmosphere and the prospects for developing regulatory controls. *Atmospheric Environment*, *44*(39), 5035–5052. <https://doi.org/10.1016/j.atmosenv.2010.08.016>
- Lee, B. P., Li, Y. J., Flagan, R. C., Lo, C., & Chan, C. K. (2013). Sizing characterization of the fast mobility particle sizer (FMPS) against SMPS and HR-ToF-AMS. *Aerosol Science and Technology*, *47*(9), 1030–1037. <https://doi.org/10.1080/02786826.2013.810809>
- Lee, S. H., Gordon, H., Yu, H., Lehtipalo, K., Haley, R., Li, Y., & Zhang, R. (2019). New particle formation in the atmosphere: From molecular clusters to global climate. *Journal of Geophysical Research: Atmospheres*, *124*, 7098–7146. <https://doi.org/10.1029/2018JD029356>
- Li, K., Zhu, Y. J., Gao, H. W., & Yao, X. H. (2015). A comparative study of cloud condensation nuclei measured between non-heating and heating periods at a suburb site of Qingdao in the North China. *Atmospheric Environment*, *112*, 40–53. <https://doi.org/10.1016/j.atmosenv.2015.04.024>
- Li, X., Zhao, B., Zhou, W., Shi, H., Yin, R., Cai, R., et al. (2020). Responses of gaseous sulfuric acid and particulate sulfate to reduced SO<sub>2</sub> concentration: A perspective from long-term measurements in Beijing. *Science of the Total Environment*, *721*, 137700. <https://doi.org/10.1016/j.scitotenv.2020.137700>
- Liu, M., Huang, X., Song, Y., Xu, T., Wang, S., Wu, Z., et al. (2018). Rapid SO<sub>2</sub> emission reductions significantly increase tropospheric ammonia concentrations over the North China Plain. *Atmospheric Chemistry and Physics*, *18*(24), 17933–17943. <https://doi.org/10.5194/acp-18-17933-2018>
- Liu, S., Hu, M., Wu, Z. J., Wehner, B., Wiedensohler, A., & Cheng, Y. F. (2008). Aerosol number size distribution and new particle formation at a rural/coastal site in Pearl River Delta (PRD) of China. *Atmospheric Environment*, *42*(25), 6275–6283. <https://doi.org/10.1016/j.atmosenv.2008.01.063>
- Liu, X. H., Zhu, Y. J., Zheng, M., Gao, H. W., & Yao, X. H. (2014). Production and growth of new particles during two cruise campaigns in the marginal seas of China. *Atmospheric Chemistry and Physics*, *14*, 7941–7951. <https://doi.org/10.5194/acp-14-7941-2014>
- Ma, L., Zhu, Y., Zheng, M., Sun, Y., Huang, L., Liu, X., et al. (2021). Investigating three patterns of new particles growing to the size of cloud condensation nuclei in Beijing's urban atmosphere. *Atmospheric Chemistry and Physics*, *21*, 183–200. <https://doi.org/10.5194/acp-21-183-2021>
- Ma, N., Zhao, C., Tao, J., Wu, Z., Kecorius, S., Wang, Z., et al. (2016). Variation of CCN activity during new particle formation events in the North China Plain. *Atmospheric Chemistry and Physics*, *16*(13), 8593–8607. <https://doi.org/10.5194/acp-16-8593-2016>
- Man, H., Zhu, Y., Ji, F., Yao, X., Lau, N. T., Li, Y., et al. (2015). Comparison of daytime and nighttime new particle growth at the HKUST supersite in Hong Kong. *Environmental Science & Technology*, *49*, 7170–7178. <https://doi.org/10.1021/acs.est.5b02143>
- McMurry, P. H., Fink, M., Sakurai, H., Stolzenburg, M. R., Mauldin, R. L., III, Smith, J., et al. (2005). A criterion for new particle formation in the sulfur rich Atlanta atmosphere. *Journal of Geophysical Research*, *110*, D22S02. <https://doi.org/10.1029/2005JD005901>
- Meng, H., Zhu, Y. J., Evans, G., & Yao, X. H. (2015). An approach to investigate new particle formation in the vertical direction on the basis of high time-resolution measurements at ground level and sea level. *Atmospheric Environment*, *102*, 366–375. <https://doi.org/10.1016/j.atmosenv.2014.12.016>
- Nieminen, T., Asmi, A., Dal Maso, M., Aalto, P. P., Keronen, P., Petäjä, T., et al. (2014). Trends in atmospheric new-particle formation: 16 years of observations in a boreal-forest environment. *Boreal Environment Research*, *19*, 191–214.
- Nieminen, T., Manninen, H. E., Sihto, S. L., Yli-Juuti, T., Mauldin, R. L., III, Petäjä, T., et al. (2009). Connection of sulfuric acid to atmospheric nucleation in boreal forest. *Environmental Science & Technology*, *43*, 4715–4721. <https://doi.org/10.1021/es803152j>
- O'Dowd, C. D., Jimenez, J. L., Bahreini, R., Flagan, R. C., Seinfeld, J. H., Hämeri, K., et al. (2002). Marine aerosol formation from biogenic iodine emissions. *Nature*, *417*(6889), 632–636. <https://doi.org/10.1038/nature00775>
- Peng, J. F., Hu, M., Wang, Z. B., Huang, X. F., Kumar, P., Wu, Z. J., et al. (2014). Submicron aerosols at thirteen diversified sites in China: Size distribution, new particle formation and corresponding contribution to cloud condensation nuclei production. *Atmospheric Chemistry and Physics*, *14*, 10249–10265. <https://doi.org/10.5194/acp-14-10249-2014>
- Petters, M. D., & Kreidenweis, S. M. (2007). A single parameter representation of hygroscopic growth and cloud condensation nucleus activity. *Atmospheric Chemistry and Physics*, *7*(8), 1961–1971. <https://doi.org/10.5194/acp-7-1961-2007>
- Qi, X. M., Ding, A. J., Nie, W., Petäjä, T., Kerminen, V.-M., Herrmann, E., et al. (2015). Aerosol size distribution and new particle formation in the western Yangtze River Delta of China: 2 years of measurements at the SORPES station. *Atmospheric Chemistry and Physics*, *15*, 12445–12464. <https://doi.org/10.5194/acp-15-12445-2015>
- Riipinen, I., Yli-Juuti, T., Pierce, J. R., Petäjä, T., Worsnop, D. R., Kulmala, M., & Donahue, N. M. (2012). The contribution of organics to atmospheric nanoparticle growth. *Nature Geoscience*, *5*(7), 453–458. <https://doi.org/10.1038/ngeo1499>
- Saha, P. K., Robinson, E. S., Shah, R. U., Zimmerman, N., Apte, J. S., Robinson, A. L., & Presto, A. A. (2018). Reduced ultrafine particle concentration in urban air: Changes in nucleation and anthropogenic emissions. *Environmental Science & Technology*, *52*, 6798–6806. <https://doi.org/10.1021/acs.est.8b00910>
- Schlesinger, R. B., Kunzli, N., Hidy, G. M., Gotschi, T., & Jerrett, M. (2006). The health relevance of ambient particulate matter characteristics: Coherence of toxicological and epidemiological inferences. *Inhalation Toxicology*, *18*(2), 95–125. <https://doi.org/10.1080/08958370500306016>
- Seinfeld, J. H., & Pandis, S. N. (2012). *Atmospheric chemistry and physics: From air pollution to climate change*. New York: John Wiley & Sons.
- Shen, L., Wang, H., Lü, S., Li, L., Yuan, J., Zhang, X., et al. (2016). Observation of aerosol size distribution and new particle formation at a coastal city in the Yangtze River Delta, China. *Science of the Total Environment*, *565*, 1175–1184. <https://doi.org/10.1016/j.scitotenv.2016.05.164>
- Shen, X., Sun, J., Zhang, Y., Wehner, B., Nowak, A., Tuch, T., et al. (2011). First long-term study of particle number size distributions and new particle formation events of regional aerosol in the North China Plain. *Atmospheric Chemistry and Physics*, *11*, 1565–1580. <https://doi.org/10.5194/acp-11-1565-2011>
- Shi, J., Wang, N., Gao, H., Baker, A. R., Yao, X., & Zhang, D. (2019). Phosphorus solubility in aerosol particles related to particle sources and atmospheric acidification in Asian continental outflow. *Atmospheric Chemistry and Physics*, *19*, 847–860. <https://doi.org/10.5194/acp-19-847-2019>
- Sihto, S.-L., Kulmala, M., Kerminen, V.-M., Dal Maso, M., Petäjä, T., Riipinen, I., et al. (2006). Atmospheric sulphuric acid and aerosol formation: Implications from atmospheric measurements for nucleation and early growth mechanisms. *Atmospheric Chemistry and Physics*, *6*, 4079–4091. <https://doi.org/10.5194/acp-6-4079-2006>
- Sipilä, M., Sarnela, N., Jokinen, T., Henschel, H., Junninen, H., Kontkanen, J., et al. (2016). Molecular-scale evidence of aerosol particle formation via sequential addition of HIO<sub>3</sub>. *Nature*, *537*, 532–534. <https://doi.org/10.1038/nature19314>

- Stangl, C. M., Krasnomowitz, J. M., Apsokardu, M. J., Tiszenkel, L., Ouyang, Q., Lee, S., & Johnston, M. V. (2019). Sulfur dioxide modifies aerosol particle formation and growth by ozonolysis of monoterpenes and isoprene. *Journal of Geophysical Research: Atmospheres*, 124(8), 4800–4811. <https://doi.org/10.1029/2018JD030064>
- Teng, X., Hu, Q., Zhang, L., Qi, J., Shi, J., Xie, H., et al. (2017). Identification of major sources of atmospheric NH<sub>3</sub> in an urban environment in northern China during wintertime. *Environmental Science & Technology*, 51, 6839–6848. <https://doi.org/10.1021/acs.est.7b00328>
- Tröstl, J., Chuang, W. K., Gordon, H., Heinritzi, M., Yan, C., Molteni, U., et al. (2016). The role of low-volatility organic compounds in initial particle growth in the atmosphere. *Nature*, 533, 527–531. <https://doi.org/10.1038/nature18271>
- Vu, T. V., Delgado-Saborit, J. M., & Harrison, R. M. (2015). Review: Particle number size distributions from seven major sources and implications for source apportionment studies. *Atmospheric Environment*, 122, 114–132. <https://doi.org/10.1016/j.atmosenv.2015.09.027>
- Wang, H., Wu, Q. Z., Guenther, A. B., Yang, X. C., Wang, L. N., Xiao, T., et al. (2021). A long-term estimation of biogenic volatile organic compound (BVOC) emission in China from 2001–2016: The roles of land cover change and climate variability. *Atmospheric Chemistry and Physics*, 21(6), 4825–4848. <https://doi.org/10.5194/acp-21-4825-2021>
- Wang, J., Feng, L., Palmer, P. I., Liu, Y., Fang, S., Bösch, H., et al. (2020). Large Chinese land carbon sink estimated from atmospheric carbon dioxide data. *Nature*, 586, 720–723. <https://doi.org/10.1038/s41586-020-2849-9>
- Wang, M., Kong, W., Marten, R., He, X., Chen, D., Pfeifer, J., et al. (2020). Rapid growth of new atmospheric particles by nitric acid and ammonia condensation. *Nature*, 581, 184–189. <https://doi.org/10.1038/s41586-020-2270-4>
- Wang, T., Wang, P., Theys, N., Tong, D., Hendrick, F., Zhang, Q. (2018). Spatial and temporal changes in SO<sub>2</sub> regimes over China in the recent decade and the driving mechanism. *Atmospheric Chemistry and Physics*, 18, 18063–18078. <https://doi.org/10.5194/acp-18-18063-2018>
- Wang, Y., Hopke, P. K., Chalupa, D. C., & Utell, M. J. (2011). Long-term study of urban ultrafine particles and other pollutants. *Atmospheric Environment*, 45, 7672–7680. <https://doi.org/10.1016/j.atmosenv.2010.08.022>
- Wang, Z. B., Birmili, W., Hamed, A., Wehner, B., Spindler, G., Pei, X. Y., et al. (2017). Contributions of volatile and nonvolatile compounds (at 300°C) to condensational growth of atmospheric nanoparticles: An assessment based on 8.5 years of observations at the central Europe background site Melpitz. *Journal of Geophysical Research: Atmospheres*, 122, 485–497. <https://doi.org/10.1002/2016JD025581>
- Wang, Z. B., Hu, M., Sun, J. Y., Yue, D. L., Shen, X. J., Zhang, Y. M., et al. (2013). Characteristics of regional new particle formation in urban and regional background environments in the North China Plain. *Atmospheric Chemistry and Physics*, 13(24), 12495–12506. <https://doi.org/10.5194/acp-13-12495-2013>
- Wehner, B., Wiedensohler, A., Tuch, T. M., Wu, Z. J., Hu, M., Slanina, J., & Kiang, C. S. (2004). Variability of the aerosol number size distribution in Beijing, China: New particle formation, dust storms, and high continental background. *Geophysical Research Letters*, 31, L22108. <https://doi.org/10.1029/2004GL021596>
- Wiedensohler, A., Cheng, Y. F., Nowak, A., Wehner, B., Achtert, P., Berghof, M., et al. (2009). Rapid aerosol particle growth and increase of cloud condensation nucleus activity by secondary aerosol formation and condensation: A case study for regional air pollution in north-eastern China. *Journal of Geophysical Research: Atmospheres*, 114, D00G08. <https://doi.org/10.1029/2008JD010884>
- Wu, Z. J., Hu, M., Lin, P., Liu, S., Wehner, B., & Wiedensohler, A. (2008). Particle number size distribution in the urban atmosphere of Beijing, China. *Atmospheric Environment*, 42(34), 7967–7980. <https://doi.org/10.1016/j.atmosenv.2008.06.022>
- Wu, Z. J., Hu, M., Liu, S., Wehner, B., Bauer, S., Maßling, A., et al. (2007). New particle formation in Beijing, China: Statistical analysis of a 1-year data set. *Journal of Geophysical Research*, 112, D09209. <https://doi.org/10.1029/2006JD007406>
- Xiao, Q. Y., Ma, Z. W., Li, S. S., & Liu, Y. (2015). The impact of winter heating on air pollution in China. *PLoS One*, 10(1), e0117311. <https://doi.org/10.1371/journal.pone.0117311>
- Yao, L., Garmash, O., Bianchi, F., Zheng, J., Yan, C., Kontkanen, J., et al. (2018). Atmospheric new particle formation from sulfuric acid and amines in a Chinese megacity. *Science*, 361, 278–281. <https://doi.org/10.1126/science.aao4839>
- Yao, X. H., Lau, N. T., Fang, M., & Chan, C. K. (2005). Real-time observation of the transformation of ultrafine atmospheric particle modes. *Aerosol Science and Technology*, 39(9), 831–841. <https://doi.org/10.1080/02786820500295248>
- Yu, F., & Luo, G. (2009). Simulation of particle size distribution with a global aerosol model: Contribution of nucleation to aerosol and CCN number concentrations. *Atmospheric Chemistry and Physics*, 9, 7691–7710. <https://doi.org/10.5194/acp-9-7691-2009>
- Yu, H., Ren, L. L., Huang, X. P., Xie, M. J., He, J., Xiao, H., et al. (2019). Iodine speciation and size distribution in ambient aerosols at a coastal new particle formation hotspot in China. *Atmospheric Chemistry and Physics*, 19(6), 4025–4039. <https://doi.org/10.5194/acp-19-4025-2019>
- Yue, D. L., Hu, M., Wu, Z. J., Wang, Z. B., Guo, S., Wehner, B., et al. (2009). Characteristics of aerosol size distributions and new particle formation in the summer in Beijing. *Journal of Geophysical Research*, 114, D00G12. <https://doi.org/10.1029/2008JD010894>
- Yue, D. L., Hu, M., Zhang, R. Y., Wu, Z. J., Su, H., Wang, Z. B., et al. (2011). Potential contribution of new particle formation to cloud condensation nuclei in Beijing. *Atmospheric Environment*, 45(33), 6070–6077. <https://doi.org/10.1016/j.atmosenv.2011.07.037>
- Zhang, C., Ito, A., Shi, Z., Aita, M., Yao, X., Chu, Q., et al. (2019). Fertilization of the northwest Pacific Ocean by East Asia air pollutants. *Global Biogeochemical Cycles*, 33(6), 690–702. <https://doi.org/10.1029/2018GB006146>
- Zhang, R., Khalizov, A., Wang, L., Hu, M., & Xu, W. (2012). Nucleation and growth of nanoparticles in the atmosphere. *Chemical Reviews*, 112(3), 1957–2011. <https://doi.org/10.1021/cr2001756>
- Zhang, R., Wang, G., Guo, S., Zamora, M. L., Ying, Q., Lin, Y., et al. (2015). Formation of urban fine particulate matter. *Chemical Reviews*, 115(10), 3803–3855. <https://doi.org/10.1021/acs.chemrev.5b00067>
- Zhang, X. D., Huang, T., Zhang, L. M., Shen, Y. J., Zhao, Y., Gao, H., et al. (2016). Three-North Shelter Forest Program contributions to long-term increasing trends of biogenic isoprene emission in northern China. *Atmospheric Chemistry and Physics*, 16(11), 6949–6960. <https://doi.org/10.5194/acp-16-6949-2016>
- Zheng, B., Tong, D., Li, M., Liu, F., Hong, C., Geng, G., et al. (2018). Trends in China's anthropogenic emissions since 2010 as the consequence of clean air actions. *Atmospheric Chemistry and Physics*, 18(19), 14095–14111. <https://doi.org/10.5194/acp-18-14095-2018>
- Zheng, C., Shen, J., Zhang, Y., Huang, W., Zhu, X., Wu, X., et al. (2017). Quantitative assessment of industrial VOC emissions in China: Historical trend, spatial distribution, uncertainties, and projection. *Atmospheric Environment*, 150, 116–125. <https://doi.org/10.1016/j.atmosenv.2016.11.023>
- Zhou, Y., Dada, L., Liu, Y., Fu, Y., Kangasluoma, J., Chan, T., et al. (2020). Variation of size-segregated particle number concentrations in wintertime Beijing. *Atmospheric Chemistry and Physics*, 20, 1201–1216. <https://doi.org/10.5194/acp-20-1201-2020>
- Zhu, Y., Hinds, W. C., Kim, S., & Sioutas, C. (2002). Concentration and size distribution of ultrafine particles near a major highway. *Journal of the Air & Waste Management Association*, 52, 1032–1042. <https://doi.org/10.1080/10473289.2002.10470842>
- Zhu, Y. J., Li, K., Shen, Y. J., Gao, Y., Liu, X. H., Yu, Y., et al. (2019). New particle formation in the marine atmosphere during seven cruise campaigns. *Atmospheric Chemistry and Physics*, 19(1), 89–113. <https://doi.org/10.5194/acp-19-89-2019>

- Zhu, Y. J., Sabaliauskas, K., Liu, X. H., Meng, H., Gao, H. W., Jeong, C. H., et al. (2014). Comparative analysis of new particle formation events in less and severely polluted urban atmosphere. *Atmospheric Environment*, *98*, 655–664. <https://doi.org/10.1016/j.atmosenv.2014.09.043>
- Zhu, Y. J., Xue, L. K., Gao, J., Chen, J. M., Li, H. Y., Zhao, Y., et al. (2021). Increased new particle yields with largely decreased probability of survival to CCN size at the summit of Mt. Tai under reduced SO<sub>2</sub> emissions. *Atmospheric Chemistry and Physics*, *21*(2), 1305–1323. <https://doi.org/10.5194/acp-21-1305-2021>
- Zhu, Y. J., Yan, C. Q., Zhang, R. Y., Wang, Z. F., Zheng, M., Gao, H. W., et al. (2017). Simultaneous measurements of new particle formation at 1 s time resolution at a street site and a rooftop site. *Atmospheric Chemistry and Physics*, *17*(15), 9469–9484. <https://doi.org/10.5194/acp-17-9469-2017>
- Zimmerman, N., Jeong, C. H., Wang, J. M., Ramos, M., Wallace, J. S., & Evans, G. J. (2015). A source-independent empirical correction procedure for the fast mobility and engine exhaust particle sizers. *Atmospheric Environment*, *100*, 178–184. <https://doi.org/10.1016/j.atmosenv.2014.10.054>

## References From the Supporting Information

- Kulmala, M., Dal Maso, M., Mäkelä, J. M., Pirjola, L., Väkevä, M., Aalto, P., et al. (2001). On the formation, growth and composition of nucleation mode particles. *Tellus B: Chemical and Physical Meteorology*, *53*(4), 479–490. <https://doi.org/10.1034/j.1600-0889.2001.530411.x>
- Whitby, K. T. (1978). The physical characteristics of sulfur aerosols. *Atmospheric Environment*, *12*(1–3), 135–159. [https://doi.org/10.1016/0004-6981\(78\)90196-8](https://doi.org/10.1016/0004-6981(78)90196-8)